Validation fire tests on using the adiabatic surface temperature for predicting heat transfer

Ulf Wickström
Robert Jansson
Heimo Tuovinen

SP Technical Research Institute of Sweden

BRANDFORSK
Styrelsen för svensk brandforskning

Projekt nr 310-081

Fire Technology

SP Report 2009:19

Validation fire tests on using the adiabatic surface temperature for predicting heat transfer

Ulf Wickström
Robert Jansson
Heimo Tuovinen

Abstract

In this report it is shown how temperature measurements with plate thermometers, PTs, as defined in the international fire resistance furnace test standard ISO 834, can be used for predicting heat transfer and temperature in fire exposed structures. To verify the theory, experiments were conducted in a small room with dimensions as given in the Room/Corner standard ISO 9705, i.e., 3.6 m by 2.4 m and 2.4 m high with a door opening. In the tests a steel beam was hanging 20 cm below the ceiling along the centre of the room. A gas burner yielding a constant heat output of 450 kW was placed in one corner, 0.65 m above the floor level. Temperatures were measured in the gas phase with various thermocouples including plate thermometers as well as in the steel beams. The measurements were made on all four sides of the beam at three locations along the beam. As the gas phase temperature and radiation fields were very inhomogeneous the recorded temperatures varied considerably depending on location and direction as well as on time.

In the report it is shown how the so called adiabatic surface temperature, AST, can be calculated from the PT readings. Temperatures in the steel beam at various positions were then calculated with the finite element computer code, Tasef, with heat flux boundary conditions derived from the ASTs. Comparisons between calculated and measured steel temperatures were very good which proves that the PT measurements in combination with the adiabatic surface temperature concept gives an accurate measure of the level of thermal exposure.

Key words: plate thermometer, heat transfer, temperature, calculation, measurement, finite element, Tasef

SP Sveriges Tekniska Forskningsinstitut
SP Technical Research Institute of Sweden

SP Report 2009:19
ISBN 978-91-86319-03-8
ISSN 0284-5172
Borås

Contents

Preface

The tests reported here have been sponsored by Brandforsk, the Board of Swedish Fire research, (Project 310-081) and by SP. The tests performed have been discussed within Forum - a group of the Directors of fire research organizations throughout the world. Similar tests will be carried out in a fire resistance furnace at NRC, Canada and in a Room/Corner Test facility at Branz, New Zealand.

These tests was carried out primarily for validating the a model for the use of plate thermometer measurements to calculate adiabatic surface temperatures and based on these temperatures the heat transfer to a fire exposed surfaces. The test results can also be used for evaluating CFD models like FDS. Some material data is, therefore, provided in support of modellers although this data has not been used in the calculations reported here. Some of the data are well known or measured while others are essentially accurate estimates. For the calculations reported here, input data (boundary conditions and material properties) were used as recommended in Eurocode 1 and 3 whenever appropriate.

Test data can be obtained in MS-Excel format on request from the authors.

Summary

In this report it is shown how temperature measurements with plate thermometers PTs, as defined in the international fire resistance furnace test standard ISO 834, can be used for predicting heat transfer to and temperature in fire exposed structures. To validate the theory, experiments were conducted in a small room with dimensions as given in the Room/Corner standard ISO 9705. A steel beam was suspended below the ceiling along the centre of the room,and a gas burner yielding a constant heat output of approximately 450 kW was placed in one of the corners or centred at the rear wall. The beam was either a rectangular tube filled with an insulation material (one test) or an I-beam (two tests). Temperatures were measured at three locations along the beam in the gas phase on the four sides of the beam with various types of thermocouples and with plate thermometers and in the steel beams with thermocouples peened into drilled holes. As the temperature field was very inhomogeneous the recorded temperatures varied considerably as a function of both location and time.

Three test were carried out. So called Adiabatic Surface Temperatures, ASTs, were calculated from plate thermometer recordings. Steel temperatures were then predicted with the finite element code, Tasef, using the ASTs as the only boundary conditions. Good agreement between the measured and calculated steel temperatures was obtained showing that measurements with the robust plate thermometers and the concept of an AST work well, even in highly inhomogeneous temperature fields as in the scenario studied. Any alternative methods for defining and measuring input boundary conditions would most likely yield less accurate results and not be as inexpensive and easy to perform.

The supporting theory on the use of the adiabatic surface temperature for defining thermal boundary conditions is presented in the report.

1 Introduction

A basic and common understanding of heat transfer to solids exposed to fire conditions is very important for the advancement of fire safety engineering in areas such as the prediction of the temperature and load bearing capacity of structural components as well as the time to ignition and burning characteristics of materials and products. However, because researchers and test standard developers have different ways of expressing and measuring the various forms of convection and radiation heat flux, confusion often arises.

Fire exposure conditions of structures are often characterized by small thermocouple gas temperature measurements. These yield very crude approximations of fire exposure, however, as small thermocouples yield temperatures near the gas temperature while the heat transfer to a fire exposed surface depends to a large degree on the incident radiation level, in particular under post-flashover conditions. A more useful method for characterizing the thermal insult of a fire is to measure the temperature with a thermocouple with a surface similar in terms of emissivity, size and orientation to the specimen surface being considered. The so called Plate Thermometer (PT) was developed in an effort to produce such a measurement device. It has been introduced into the international fire resistance standard ISO 834 as well as in the European standard EN 1363 Part 1 after comprehensive comparative tests in several European fire resistance furnaces [1] which proved its usefulness in characterising the thermal insult afforded a test specimen in a standardised test.

Calculating heat transfer to a fire exposed structure is in general complex. It depends on both radiation and convection conditions. Therefore simplified methods are needed. In e.g. Eurocode 1 [8] a simple formula is given concerning how to calculate the heat transfer by radiation and convection to a fire exposed structure when uniform fire temperatures are assumed. However, in fire real situations the temperature is not uniform and the gas temperature and the effective radiation temperature are not equal. It has therefore been suggested that the fire temperature in the Eurocode may be replaced by a characteristic temperature called the Adiabatic Surface Temperature AST [6,2]. Indeed the plate thermometer yields approximately the AST under standard fire test conditions according to ISO 834-1 or EN 1363-1. However, it should be noted that during rapid fire temperature development a time lag occurs during the first few minutes due to the thermal inertia of the PT.

Three experiments were performed in a small room with the main aim of validating the theory of using PT measurements and the concept of the AST for predicting heat transfer to fire exposed structures. In the experiments a steel beam was suspended 20 cm below the ceiling and a gas burner yielding a constant heat output was placed in one corner. Temperatures were measured in the gas phase,10 cm from the beam with various thermocouples including PTs as well as in the steel beams with quick tip thermocouples fixed by a punch mark (peened) in drilled holes. The measurements were made on all four sides of the beam at three locations along the beam, as the temperature field was very inhomogeneous the recorded temperatures varied considerably depending on location. There are two reasons for using a steel beam. One is that temperature can accurately be measured in such a structure, in particular the surface temperature. The other is that the temperature distribution in a steel structure can relatively easily be predicted with numerical methods given that the boundary conditions are known and well defined.

Based on the temperatures recorded by the PTs, temperatures in the steel beam at various positions were calculated with the two-dimensional finite element computer code Tasef. More simple calculation methods assuming uniform steel temperature could not be used due to the inhomogeneous boundary conditions and the non-uniform temperature fields that develops in the steel sections.

To further demonstrate the ability of PT measurement to be used for the calculation of the temperature of structural elements, tests have been carried out in a fire resistance furnace at NRC, Canada [3]. These tests have, however, not yet been analysed and published (March 2009).

2 Theory of heat transfer to structures

The heat transfer theory outlined below follows standard principals as can be found in textbooks, see e.g. Holman [5]. Heat transfer theories adapted to fire resistance problems can be found in e.g. the 4th edition of the SFPE Handbook of Fire Protection Engineering [4].

2.1 Basic theory

Heat is transferred to fire exposed structures by convection and radiation. The contributions of these two modes of heat transfer are in principal independent and must be treated separately. The convective heat transfer depends on the temperature difference, between the target surface and the surrounding gas, and the velocity of the gas masses in the vicinity of the exposed surface. The incident heat radiation on a surface originates from surrounding flames and gas masses as well as other surrounding surfaces.

Thus the total heat flux $\dot{q}''_{tot}$ to a surface is

$$\dot{q}''_{tot} = \dot{q}''_{rad} + \dot{q}''_{con} \qquad \text{Eq. 1}$$

where $\dot{q}''_{rad}$ is the net radiation heat flux and $\dot{q}''_{con}$ the heat transfer to the surface by convection. Details of these two contributions which both can be either positive or negative are given below.

2.1.1 Radiation

The heat exchange by radiation at a surface is illustrated by Figure 1. The net heat absorbed, $\dot{q}''_{rad}$, depends on the incident radiation, $\dot{q}''_{inc}$, the surface emissivity/ absorptivity and the absolute temperature, T_s, of the targeted surface to the fourth power.

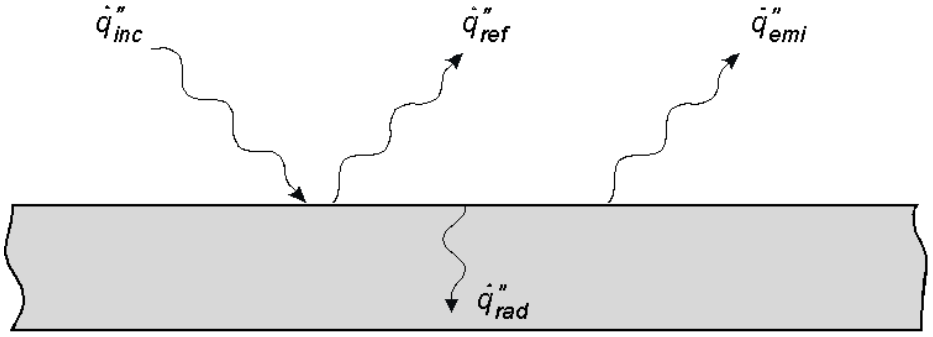

Figure 1 **The heat transfer by radiation to a surface depends on incident radiation and the surface absolute temperature and the surface emissivity.**

Part of the incident radiation is absorbed and the rest, $\dot{q}''_{ref}$, is reflected. Then the surface emits heat by radiation, $\dot{q}''_{emi}$, depending of the emissivity and the surface absolute temperature to the fourth power. Thus the net radiation heat or the heat that is absorbed by the surface can be written:

$$\dot{q}''_{rad} = \alpha_s \dot{q}''_{inc} - \varepsilon_s \sigma T_s^4 \qquad \text{Eq. 2}$$

where α_s and ε_s are the target surface absorptivity and emissivity, respectively. In this presentation the surface emissivity and absorptivity are assumed equal according to the Kirchhoff's identity. Thus

$$\dot{q}''_{rad} = \varepsilon_s (\dot{q}''_{inc} - \sigma T_s^4) \qquad \text{Eq. 3}$$

The incident radiation to a surface is emitted by surrounding gas masses and in case of fire by flames and smoke layers, and/or by other surfaces. It depends on the fourth power of the absolute temperature. The emissivity and absorptivity of gas masses and flames increase with depth and becomes therefore more important in large scale fires than in e.g. small scale experiments. In real fires surfaces are exposed to radiation from a large number of sources (surfaces, flames, gas masses etc.) of different temperatures and emissivities. The heat fluxes are then generally very complicated to model. A simple summation of the main contributions typically yields a good estimate, i.e.

$$\dot{q}''_{inc} = \sum \varepsilon_i F_i \sigma T_i^4 \qquad \text{Eq. 4}$$

where ε_i is the emissivity of the *i*:th source. F_i and T_i are the corresponding view factor and temperature, respectively. Eq. 4 may then be inserted in Eq. 3 to obtain

$$\dot{q}''_{rad} = \varepsilon_s \sigma (\sum \varepsilon_i F_i T_i^4 - T_s^4) \qquad \text{Eq. 5}$$

or

$$\dot{q}''_{rad} = \varepsilon_s \sigma (T_r^4 - T_s^4) \qquad \text{Eq. 6}$$

where T_r is the black body radiation temperature or just the radiation temperature. T_r is a weighted average, identified as

$$T_r^4 \equiv \sum \varepsilon_i F_i T_i^4 \qquad \text{Eq. 7}$$

The emissivities as used above are surfaces properties, in principle independent of the fire conditions.

2.1.2 Convection

The heat transferred by convection from adjacent gases to a surface varies depending on adjacent gas velocities and geometries.

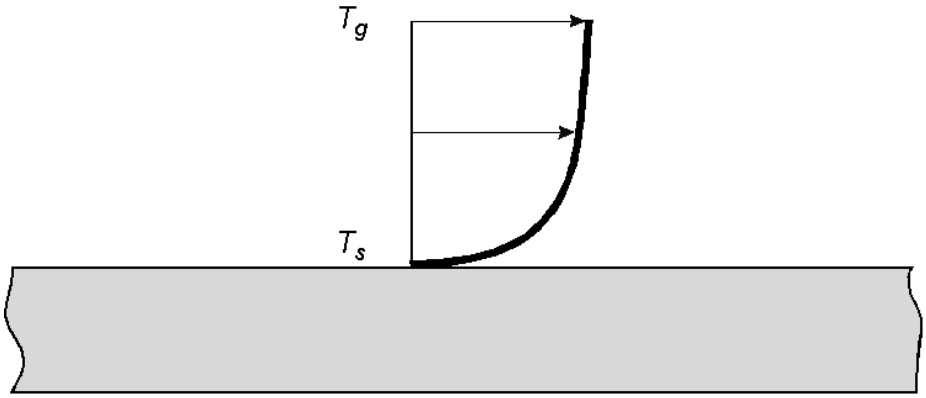

Figure 2 **Gas velocity profile. The heat transfer by convection depend on the temperature difference between the adjacent gases and the target surface, and on the gas velocity.**

In most cases it may be written as

$$\dot{q}''_{con}=h(T_g-T_s)^n \qquad \text{Eq. 8}$$

where h is the convective heat transfer coefficient and T_g is the gas temperature outside the boundary layer. In cases of surfaces heated or cooled by natural or free convection a value of n greater than unity is motivated depending on flow conditions, see textbooks such as e.g. Holman [5].

In fires the heat transfer conditions by convection may vary considerably and the parameters h and n are very hard to determine accurately. However, as radiation heat transfer dominates especially at higher temperatures and the convective conditions are not decisive for the total heat transfer to fire exposed structures, the exponent n is assumed equal to unity for simplicity in most fire engineering cases. Thus

$$\dot{q}''_{con} = h(T_g - T_s) \qquad \text{Eq. 9}$$

The convective heat transfer coefficient h depends mainly on flow conditions in the vicinity of the surface and to a minor extent on the surface or the material properties.

2.2 Total heat transfer and adiabatic surface temperature

The total heat transfer to a surface may now be obtained by adding the contributions from radiation and convection. Thus by inserting Eq. 6 and Eq. 9 into Eq. 1 the heat flux to a surface becomes

$$\dot{q}''_{tot} = \varepsilon_s\sigma(T_r^4 - T_s^4) + h(T_g - T_s) \qquad \text{Eq. 10}$$

In most fire engineering design cases the radiation temperature, T_r, and the gas temperature, T_g, are assumed equal to a fire temperature, T_f. Then the total heat transfer may be calculated as

$$\dot{q}''_{tot} = \varepsilon_s \sigma (T_f^4 - T_s^4) + h(T_f - T_s) \quad \text{Eq. 11}$$

or

$$\dot{q}''_{tot} = H(T_f - T_s) \quad \text{Eq. 12}$$

where the combined total heat transfer coefficient H may be identified from Eq. 11 and Eq. 12 as

$$H = \varepsilon_s \sigma (T_f^2 + T_s^2)(T_f + T_s) + h \quad \text{Eq. 13}$$

Alternatively the two boundary temperatures in Eq. 10,, T_r and T_g,, may be combined to one effective temperature, T_{AST}, the adiabatic surface temperature. This temperature is defined as the temperature of an ideal perfectly insulated surface when exposed to radiation and convective heat transfer [6]. Thus T_{AST} is defined by the surface heat balance equation

$$\varepsilon_s \sigma (T_r^4 - T_{AST}^4) + h(T_g - T_{AST}) = 0 \quad \text{Eq. 14}$$

The value of T_{AST} is always between T_r and T_g.

Then the total heat transfer may be written as

$$\dot{q}''_{tot} = \varepsilon_s \sigma (T_{AST}^4 - T_s^4) + h(T_{AST} - T_s) \quad \text{Eq. 15}$$

The adiabatic surface temperature, T_{AST}, can in many cases be accurately measured and it may be used for calculating heat transfer to fire exposed surfaces based on practical tests, see section 2.3 below. It can also be obtained from numerical CFD modelling of fires using computer codes like FDS [6,7].

Based on equation Eq. 11 or Eq. 12 the heat transfer to a fire exposed surface can be calculated for given fire and surface temperatures T_f and T_s. The emissivity ε_s is a surface property. In Eurocode 1 [8] a value of 0.8 is generally recommended. The convection coefficient h is not decisive for the temperature development near a fire exposed surface of a structures as the radiation heat transfer dominates at high temperatures. In Eurocode 1 [8] a value of 25 W/m^{2}K is recommended at fire exposed surfaces.

The heat transfer conditions are on the other hand very decisive for the temperature development in a fire exposed bare steel structure as being used in the experiments presented in this report.

2.3 Calculating adiabatic surface temperature and heat transfer using PT measurements

So called *plate thermometers* PTs are used to monitor the temperature in fire resistance furnaces according to the international standard ISO 834 and the European standard EN 1363-1. A plate thermometer (PT) consisting of a metal (inconel) plate insulated on its backside is shown in Figure 3. A thermocouple fixed to the metal plate registers its temperature. Figure 4 shows its position in a vertical furnace with the front side facing into the furnace and the insulated back side facing the specimen. The front side of the PT is exposed to approximately the same heating, including radiation conditions, as the

specimen. The exposed surface of the PT is relatively large and therefore its sensitivity to convective heat transfer is about the same as that of the specimen surface. The inconel plate is thin, only 0.7 mm, and responds therefore quickly to temperature changes. As a matter of fact the PT in a standard fire resistance test, measures approximately the temperature of an adiabatic surface AST, i.e. the temperature of an ideal perfect insulator exposed to the same heating conditions as the specimen surface. The effects of thermal inertia can be neglected except for the first few minutes of a standard ISO 834 fire resistance furnace test. According the standard EN 1363-1 the insulation pad of the plate thermometer shall be of an inorganic material and have a density of 280 ± 30 kg/m^2. (For more elaborate calculation purposes the specific heat capacity of the pad can be estimated to be in the order of 1000 J/kgK and the conductivity in the order of 0.1 W/mK at room temperature and increasing with temperature. Note that in the inverse calculations outlined in section 2.3.1 below , the insulation pad is assumed to be an ideal perfect insulator.) For the definition of AST see section 2.2 above.

The temperatures recorded by PTs can also be used to estimate incident radiation at high temperatures, see Ingason and Wickström [9].

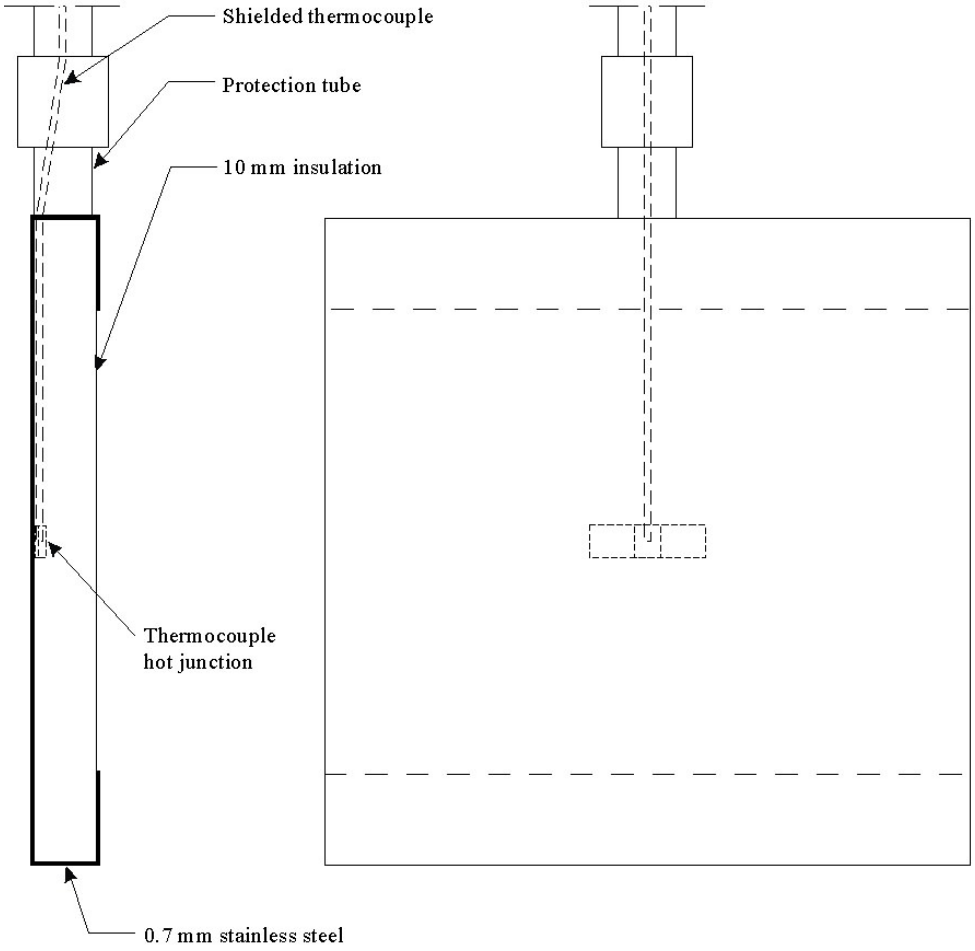

Figure 3 **A thermocouple welded to the centre of a 0.7 mm thick inconel plate insulated on its back side. The exposed front face is 100 mm by 100 mm.**

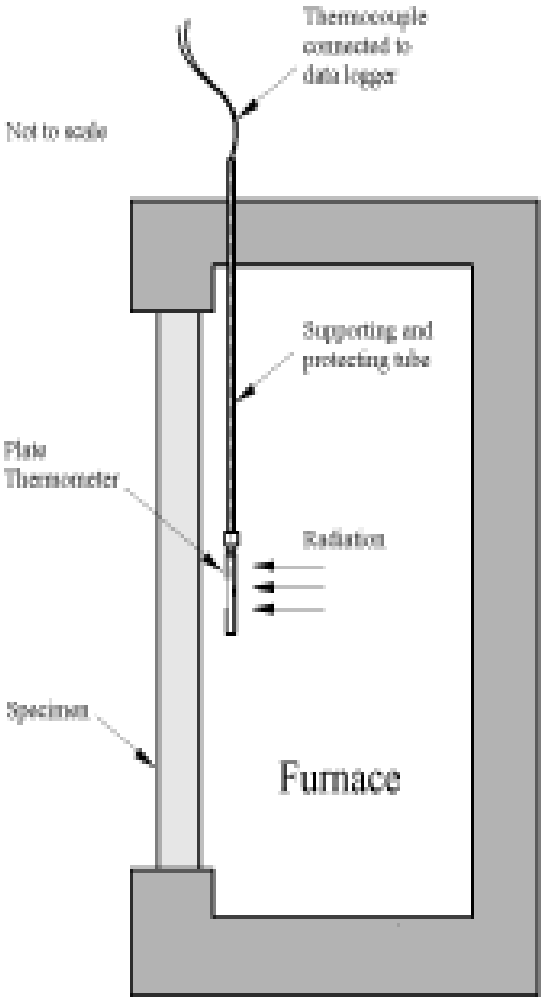

Figure 4 **The plate thermometer according to ISO 834 and EN 1363-1 placed in a fire resistance furnaces with its front side exposed to radiation from the furnace interior.**

The PT was introduced mainly to harmonize fire exposure in fire endurance tests, see ref. [10], but the measured temperatures are also well suited as input for calculating heat transfer by radiation and convection to fire exposed surfaces as will be proven by the results presented in this report.

As any surface, the PT surface exchanges heat by radiation and convection. The sum of these equals the transient heat for raising the temperature of the inconel plate and the backing insulation. Assuming that the inconel plate is thin and does not loose much heat by conduction on its back side, this implies that no significant amount of heat will be absorbed by the surface.

When neglecting the thermal inertia of the plate and the heat loss to the insulation pad, the heat balance of the plate can be written:

$$\varepsilon_{PT}(\dot{q}''_{inc} - \sigma T_{PT}^4) + h_{PT}(T_g - T_{PT}) = 0 \qquad \text{Eq. 16}$$

or

$$\varepsilon_{PT}\sigma(T_r^4 - T_{PT}^4) + h_{PT}(T_g - T_{PT}) = 0 \qquad \text{Eq. 17}$$

The index *PT* refers to plate thermometer. This means the PT yields the adiabatic temperature of the specimen for a given surface emissivity and a given convective heat transfer coefficient.

However, when the temperature rise is rapid, then the inertia of the inconel plate cannot be neglected. A simple inverse procedure on how to consider the inertia of the plate but neglecting the heat flux by conduction on the back side of the plate to the insulation pad is outlined in section 2.3.1 below.

2.3.1 Inverse calculation of adiabatic surface temperature

Given that the heat flux to the exposed side of the PT inconel plate can be written according to Eq. 10 and that the heat flux to the insulation pad on the back side may be neglected, the heat balance of the plate may be written as

$$\varepsilon_{PT}\sigma(T_{AST}^4 - T_{PT}^4) + h_{PT}(T_{AST} - T_{PT}) = c\rho d\left(\partial T_{PT} / \partial t\right) \qquad \text{Eq. 18}$$

where c, ρ and d are the specific heat capacity, density and thickness, respectively, of the inconel plate. Eq. 18 may be approximated in finite difference form as

$$c\rho d(T_{PT}^{i+1} - T_{PT}^{i})/(t^{i+1} - t^{i}) = \left[\varepsilon_s\sigma(T_{AST}^4 - T_s^4) + h(T_{AST} - T_s)\right]^i \qquad \text{Eq. 19}$$

where *t* is time and the superficies *i* and *i+1* stands for the time increment number. The T_{PT} -values are obtained by measurements and the surface emissivity ε_{PT} and the heat transfer coefficient h_{PT} must be assigned values. In the calculations reported below a surface emissivity of the PT is assumed to be 0.9 (as measured on similar surfaces) and the convective heat transfer coefficient 25 W/m^{2}K, respectively. At each time increment the value of T_{AST} is the only unknown in this equation. This type of problem of determining the exposure, in this case T_{AST}, based on the response (T_{PT}) is often named the inverse problem. Now if a function $F\left(\left[T_{AST}\right]^i\right)$ is defined at time step *i* as

$$F\left(\left[T_{AST}\right]^i\right) = \left[\varepsilon_s\sigma(T_{AST}^4 - T_s^4) + h(T_{AST} - T_s)\right]^i - c\rho d(T_{PT}^{i+1} - T_{PT}^{i})/(t^{i+1} - t^{i}) \qquad \text{Eq. 20}$$

the adiabatic or effective fire exposure temperature, T_{AST}, can be obtained at each time step for F=0. Thus the iteration formula can be derived as

$$T_{AST}^{j+1} = T_{AST}^{j} - F\left(\left[T_{AST}\right]^i\right) / F'\left(\left[T_{AST}\right]^i\right) \qquad \text{Eq. 21}$$

where *j* is the iteration step number and $F'\left(\left[T_{AST}\right]^i\right)$ is the derivative of $F\left(\left[T_{AST}\right]^i\right)$, i.e.

$$F'\left(\left[T_{AST}\right]^i\right) = 4\varepsilon_s\sigma\left[T_{AST}^3\right]^i + h \qquad \text{Eq. 22}$$

Eq. 21 may be coded into a spread sheet program like MS-Excel, and the adiabatic surface temperature can be calculated based on measured plate thermometer temperatures. Only one iteration was required to reach accurate results for the calculated ASTs reported in Appendix C - Calculated adiabatic surface temperatures .

2.3.2 Error estimate of predicted heat flux

An approximate alternative expression of the net heat transfer, $\dot{q}''_{tot}$, to a specimen surface can be obtained in terms of one effective temperature only by deducting Eq. 17 from Eq. 10:

$$\dot{q}''_{tot} = \varepsilon_s \sigma (T_{PT}^4 - T_s^4) + h(T_{PT} - T_s) \qquad \text{Eq. 23}$$

In other words the adiabatic surface temperature is approximated by the PT temperature. This rewriting of equation Eq. 10 facilitates the calculations in many cases. The error, $\Delta\dot{q}''$, introduced can be quantified by a simple algebraic analysis as:

$$\Delta\dot{q}'' = (\varepsilon_s - \varepsilon_{PT})\sigma(T_r^4 - T_{PT}^4) + (h_s - h_{PT})(T_g - T_{PT}) \qquad \text{Eq. 24}$$

Thus the error is small when the surface emissivity of the PT and the specimen are nearly the same and when the convective heat transfer coefficients are nearly the same. Therefore the surfaces of the PTs are blasted and heat treated before being used to obtain an emissivity of about 0.9. It also has a relatively large surface, 100 mm by 100 mm, to obtain a convection heat transfer coefficient similar to that of a typical specimen. As T_{pt} always has a value between T_r and T_g the error vanishes when these two temperatures are close. In such cases any fast responding thermocouple yields similar results.

3 Experiments

3.1 Test configuration

To measure the temperature response of steel beams during non-uniform heating, tests were performed inside a Room Corner test room according to the international standard ISO 9705. A Room Corner test room is 3.6 m deep, 2.4 m wide and 2.4 m high and includes a door opening 0.8 m by 2.0 m, see Figure 5. The room was constructed of 20 cm thick light weight concrete blocks with a density of 600± 100 kg/m^3 and an estimated specific heat capacity of about 800 J/kgK and a conductivity of about 0.1 W/mK.

The heat source was a gas sand burner run at a constant power of 450 kW. The top of the burner, with a square opening 30 cm by 30 cm, was placed 65 cm above the floor level 2.5 cm from the walls.

As shown in Figure 6 the burner was placed either close to the corner (Test 1 and 2) or in the centre near the rear wall directly under the beam (Test 3).

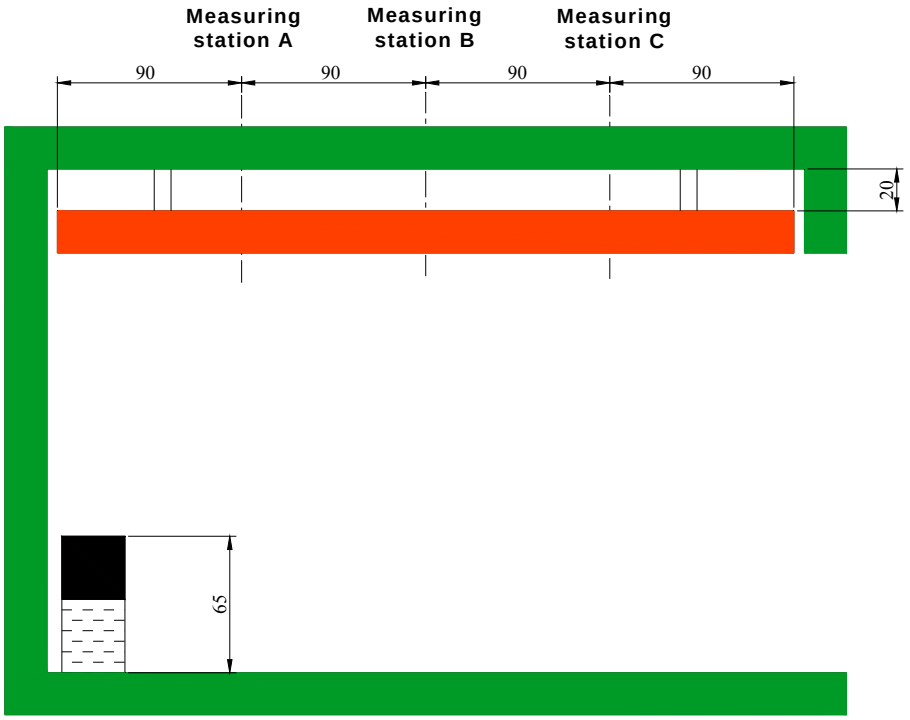

Figure 5 The ISO 9705 Room Corner Test burn room with a steel beam hanging from the ceiling (measures in cm).

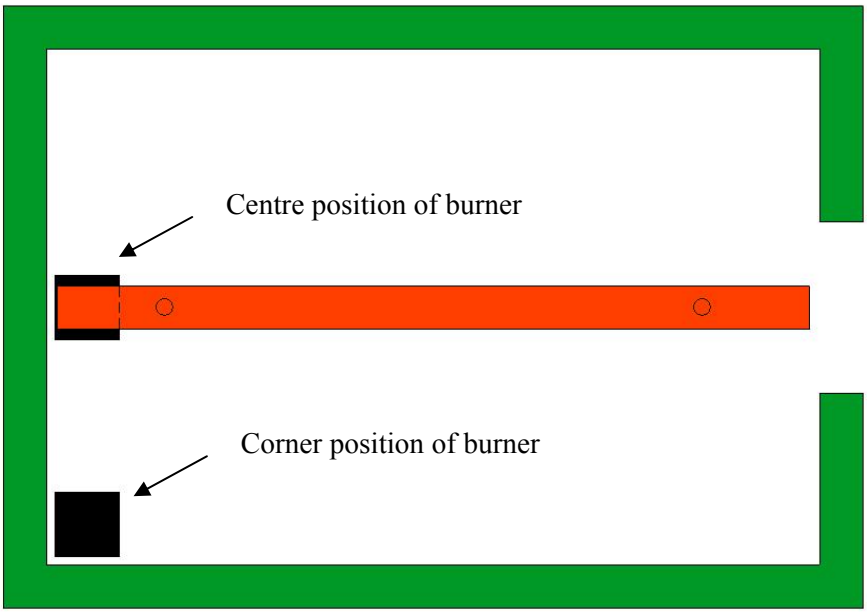

Figure 6 The two placements of the burner inside the Room Corner Test room.

Figure 7 Elevated gas burner placed in a corner of the ISO 9705 Room/Corner test room.

3.2 Steel beams

Two types of steel beams were used, an I shaped cross-section, denoted HE200B, and a hollow rectangular cross-section, denoted KKR200x100. Details concerning the cross-sections can be seen in Figure 8. During the test the beam with the hollow cross-section was filled with expanded clay pellets with a measured density of 317 kg/m^3. For the calculations a specific heat capacity of 1000 J/kgK and a conductivity of 0.1 W/m^{2}K at room temperature growing linearly to 0.2 W/m^{2}K at 1000 °C, were assumed.

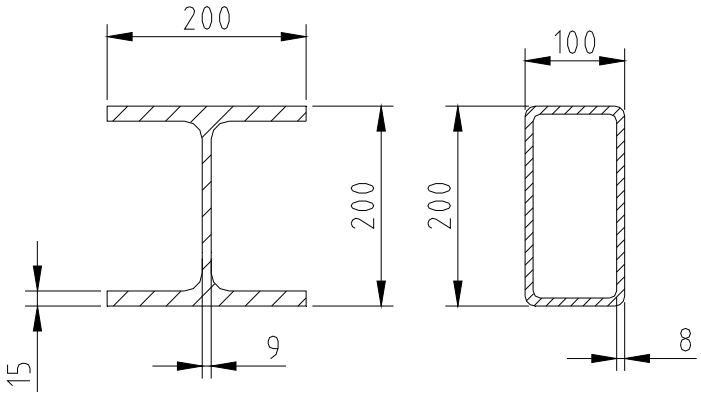

Figure 8 **Steel beam sections, HE200B and KKR200x100, respectively. Dimensions in mm.**

3.3 Measurements

Gas phase temperatures were measured with twelve plate thermometers PTs and with three types of thin thermocouples TCs, all of type K. They were all placed in four different positions/directions, 1-4 as shown in Figure 9, at the three measuring stations (A, B and C) along the beam mounted under the ceiling, see Figure 5. Thermocouples, TCs, were not placed at all positions. Depending on their shape and dimensions the TCs recorded different temperatures than the PTs due to their sensitivity to heat transfer by convection and due to their response characteristics (time constant). Photos of a plate thermometer with additional quick-tip, welded and shielded thermocouples are shown in Figure 11. The welded and quick-tip TCs had a wire diameter of 0.25 mm and the shielded TCs had an outer diameter of 1.0 mm.

Figure 12 shows quick-tip TCs placed into drilled holes and fixed by a punch mark in the nearby metal in the square section to measure steel temperatures. The position of the thermocouples for steel temperature measurement are shown in Figure 10**.**

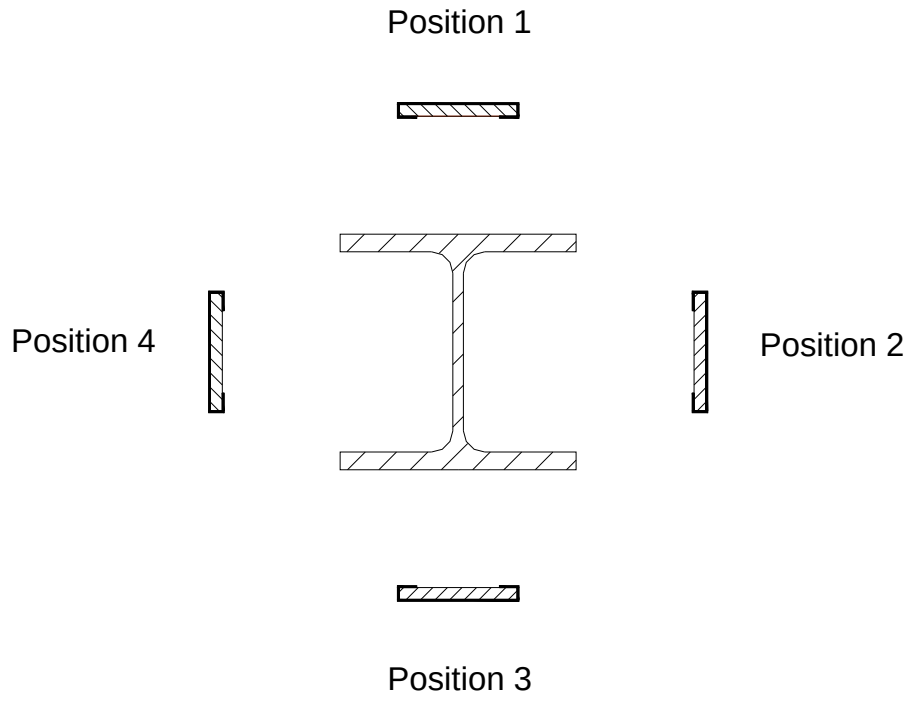

Figure 9 **Gas phase temperature thermoucouples and plate thermometers were placed 100 mm from the steal beams at positions denoted 1 to 4.**

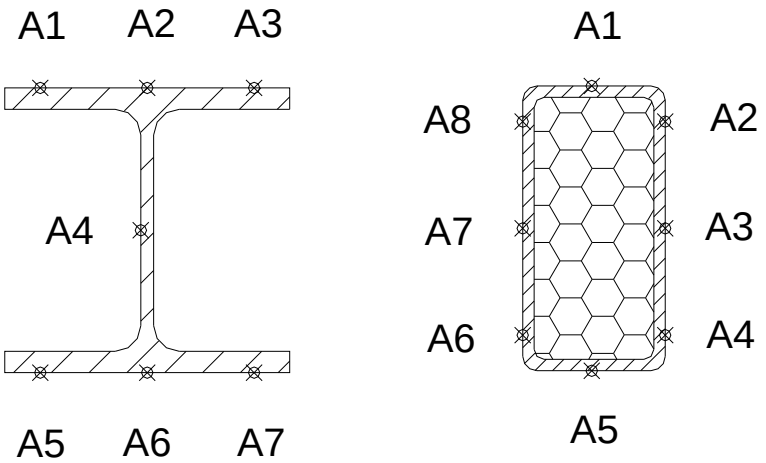

Figure 10 **Positions of thermoucouples in the steel beams (measurement position A). The corresponding position numbers apply as well to measurement positions B and C along the beams.**

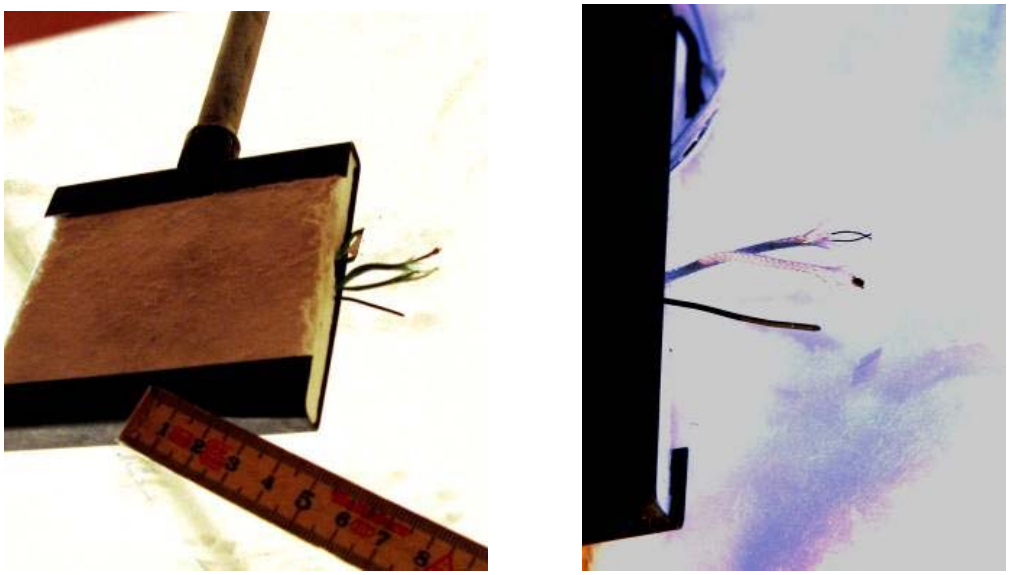

Figure 11 **Plate thermometer with additional quicktip, welded and shielded thermocouples.**

Figure 12 **Quick-tip thermocouples were peened into drilled holes in the steel. The thermocouple wires were then drawn inside the square steel beam.**

Figure 13 The plate thermometers were mounted with pipes through the ceiling. The PT thermocouple wires were drawn inside the pipes.

3.4 Performance of tests

The tests commenced with the burner run at a constant heat release rate of 450 kW in all the three tests. The burner was turned off after 30 min in Test 1 and 2. In Test 1 a fan placed in the door-way was started after 40 min to speed up the cooling rate.

As can be seen in
Figure 14 the thermal environment is very inhomogeneous with flames and high gas velocities at the top of the beam.

Figure 14 **Fire plume and square section steel beam mounted 20 cm under the ceiling. Plate thermometer aiming at four directions are mounted at three measuring stations A, B and C.**

Thus, high levels of temperature and radiation gradients were developed which make measurements and characterizations of thermal exposures or thermal insults on exposed surfaces very difficult. In practice measurements of heat radiation or total heat flux are not possible and measurements of gas temperatures with thin "normal" thermocouples yields approximate gas temperatures but little information on the incident radiation levels which is the dominating quantity governing the heat transfer to a fire exposed surface. The PT measurements were, however, shown to be very useful for predicting the heat transfer to the steel beams as was proven by the accurate predictions of the steel temperatures shown in Appendix D – Comparisons of measured and calculated steel temperatures.

4 Measured temperatures

Measured gas phase temperatures with plate thermometers and thermocouples as described in section 3.3 above are given Appendix A – Measured gas phase temperatures and the steel temperatures are shown in Appendix B – Measured steel temperatures .

Figure 19 through Figure 22 show the responses of plate thermometers and thermocouples at the four positions around the steel beam at measuring station A of Test 1 during the three phases of the experiment. First the heating phase when the burner was kept at a constant heat release rate and then during two cooling phases when the burner was shut off. In the second cooling phase a fan was placed in the door opening to speed up the cooling of the room. Note that in all cases the thermocouples responded differently than the PTs depending on their thermal inertia *and* their different sensitivity to incident radiation and gas temperature. However, the differences due to thermal inertia vanish after some minutes and the recorded temperatures depend in principle only on the current radiation and convection conditions, i.e. gas temperature and velocity. Thus above the beam (position 1, see Figure 19), where the PT is influenced by radiation from the more slowly heated ceiling surface, the PT temperature is considerably (appr. 75 ºC) lower than the TC recordings even at the end of the heating period. Similarly, below the beam (position 3, see Figure 21) where the PT is facing the cool floor the PT temperature is about 50 ºC below the TC temperatures. Note also that the temperature is rising at a considerably slower rate at position 3 than at the other positions. This is explained by the influence of the slow temperature rise of the floor surface and the relatively slow filling process of hot gases from the ceiling. On the burner side of the beam (position 4, Figure 22) the PT temperature is almost 100 ºC above the TC temperature, as the PT is exposed by radiation from the burner plume. At the other side of the beam (position 2, Figure 20) the temperature recordings are almost the same for the PT and the TCs at the end of the heating period.

A closer look at different TC time-temperature curves in for example Figure 20 shows that the welded TC (0.25 mm) responds fastest, while the quick-tip TC and the shielded TC (1.0 mm) are slightly slower and more sensitive to radiation as they record temperature closer to the PT temperatures than the welded TCs. The very small differences between the 0.5 mm and the 1.0 mm thick TCs is an indication that they are only marginally influenced by radiation and adjust to the gas temperature.

5 Measured plate thermometer temperatures and calculated adiabatic surface temperatures AST

As outlined in section 2.3.1 above the adiabatic surface temperature, AST, can be derived from the plate thermometer temperature. In these calculations a simple lumped heat capacity is assumed. The experiences of these calculations indicate that except when the temperatures change rapidly, as during the first few minutes of the tests reported here, the PT and AST are almost the same and can be assumed to be equal. Otherwise the AST must be obtained by inverse calculations as suggested here or in a more elaborate way including modelling the heat transfer to the insulation pad.

The calculated adiabatic surface temperature based on of all the measured PT temperatures are shown in Appendix C - Calculated adiabatic surface temperatures . In all these inverse calculations the surface emissivity of the PT is assumed equal 0.9 and the convection heat transfer coefficient 20 W/m^2K. The thickness, density and specific heat capacity of the PT plate are assumed equal 0.7 mm, 7800 kg/m^3 and 500 W/kg K, respectively.

Figure 15 shows measured plate thermometer temperature curves and corresponding calculated adiabatic surface temperature curves for test 1 at measuring station A, positions 1 to 4.

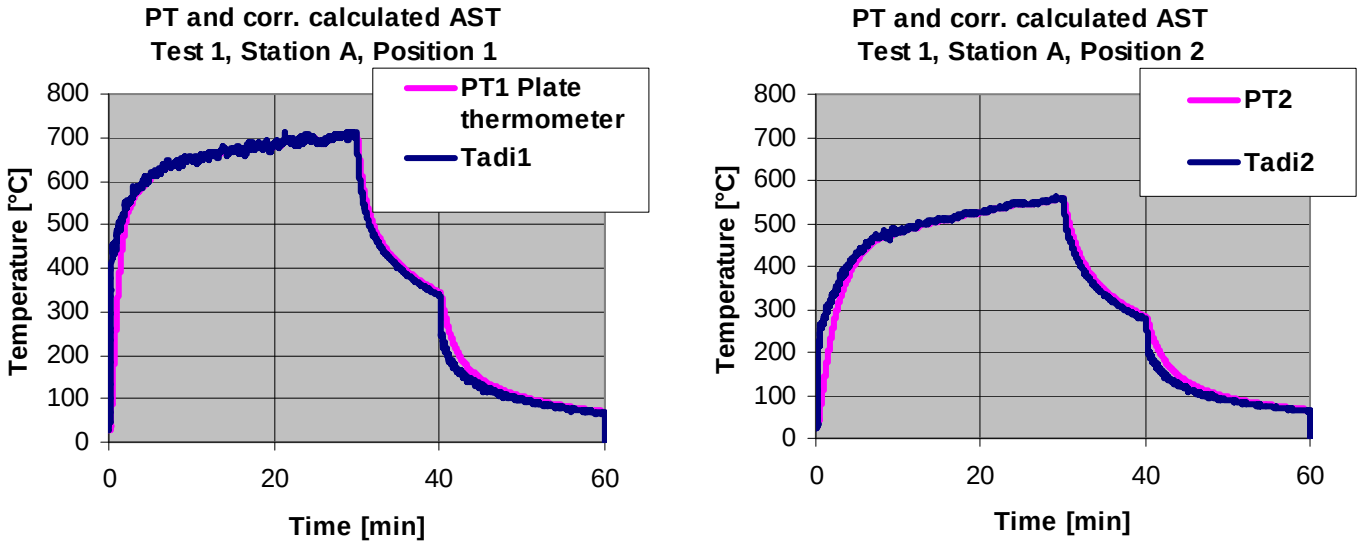

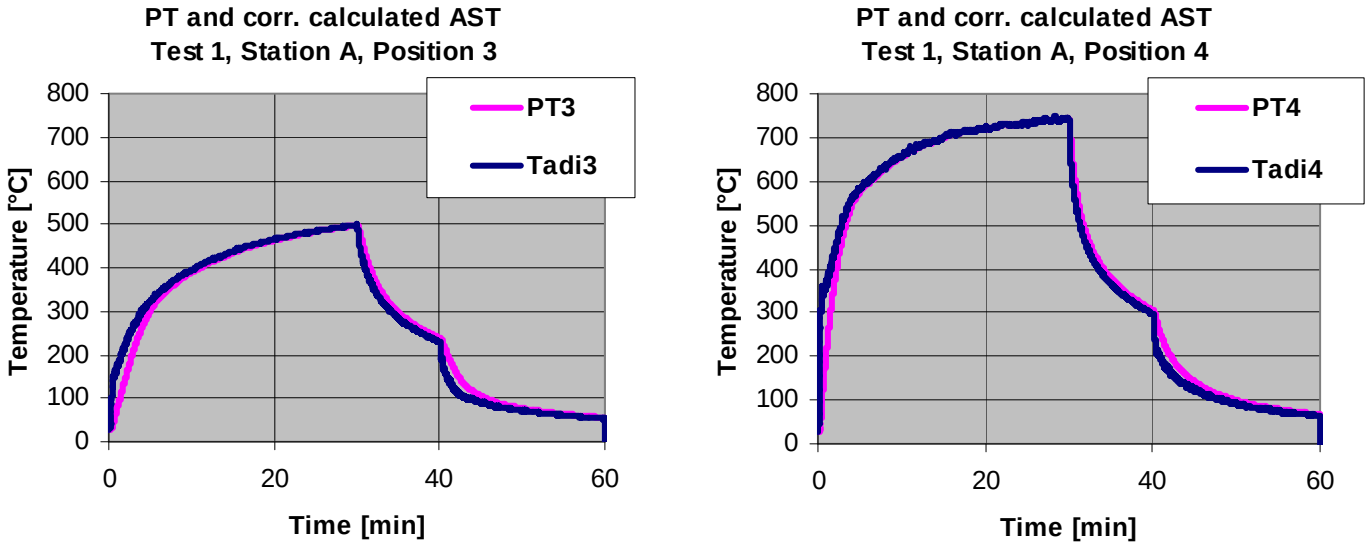

Figure 15 **Comparison between plate thermometer temperatures and adiabatic surface temperature calculated from these temperatures. Test 1, station A, position 1 – 4.**

6 Comparisons of measured and calculated steel temperatures

To demonstrate that the heat transfer to a surface by radiation and convection can be calculated based on PT measurements, the temperature of steel sections were calculated with the adiabatic surface temperature obtained from the PT measurements as the only input boundary conditions. Steel sections were used because temperature of steel is easy to measure, and it is also easy to calculate accurately given the boundary conditions are correctly defined. Thus the precision of the steel temperature predictions is a good measure of the accuracy of the given boundary condition, as the uncertainty of the measurements as well as of the temperature calculations are small given the boundary conditions are correct.

Graphs showing measure and calculated steel temperatures are shown in Appendix D – Comparisons of measured and calculated steel temperatures.

6.1 Calculations of steel temperatures using the finite element code Tasef

The temperatures of the steel beams were calculated using the 2-D finite element temperature calculation code Tasef [13]. The thermal properties of steel were assumed as given in Eurocode 3. The adiabatic surface temperatures as obtained from plate thermometer measurements as described in section 2.3 above were the only boundary conditions applied. All steel surface emissivities were assumed to be 0.7 according to Eurocode 3 [12] and all convection heat transfer coefficients were assumed to be 25 $W/m^2 K$ as recommended in Eurocode 1 [8] for fire exposed structures. Two-dimensional analyses over the steel sections were performed at each of the measuring stations. Separate AST's were assumed in the four different directions. For the I-shaped sections the shadow effects were considered, see section 6.1.2 below.

6.1.1 Rectangular hollow steel section

The rectangular steel section was modelled as shown in Figure 16. Heat transfer boundary conditions as given by Eq. 15 were applied with different adiabatic surface temperatures, T_{AST}, as a function of time assumed at four positions/sides. These temperatures were calculated based on the plate thermometer recordings adjusted for the thermal inertia according to the inverse calculation procedure outlined in section 2.3.1 above. The inside of the steel beam was filled with an inert insulation material (expanded clay pellets) to minimize heat transfer from the inner surfaces of the steel beam and thereby to facilitate the internal thermal analysis of the steel section. If the void had been empty heat exchange by radiation and convection would have occurred which would have complicated the thermal model of the steel beam and the interpretation of the test results.

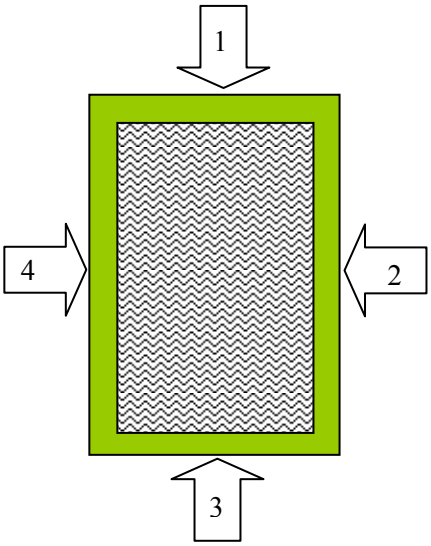

Figure 16 **Four different fire exposures expressed in terms of adiabatic surface temperatures were assumed at the four sides, respectively. The void of the beam is filled with inert insulation(expanded clay pellets).**

6.1.2 I-beam steel section – shadow effects

The over all boundary conditions of the I-beam steel section is as shown in Figure 17. However, the heat transfer by radiation to open sections like an I-shaped steel sections are interfered by the so called shadow effect as described in ref. [11] and introduced in Eurocode 3 [12]. Thus the web and the insides of the flanges are exposed not only to the radiation from the fire but also partly to the radiation from other parts of the section. This effect can be considered by assuming a virtual surface between the ends of the flanges. In the finite element analysis the artificial surface is then assumed to get a prescribed temperature equal to the adiabatic surface temperature. Then the heat transfer by radiation and convection in the enclosure between this surface, the web and the flanges can be calculated [13].

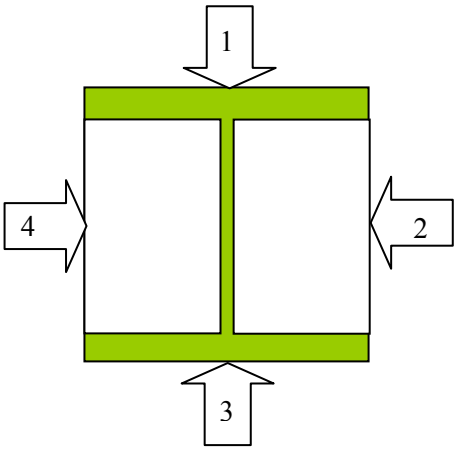

Figure 17 **Four different fire exposures expressed in terms of adiabatic surface temperatures were assumed at the four sides, respectively.**

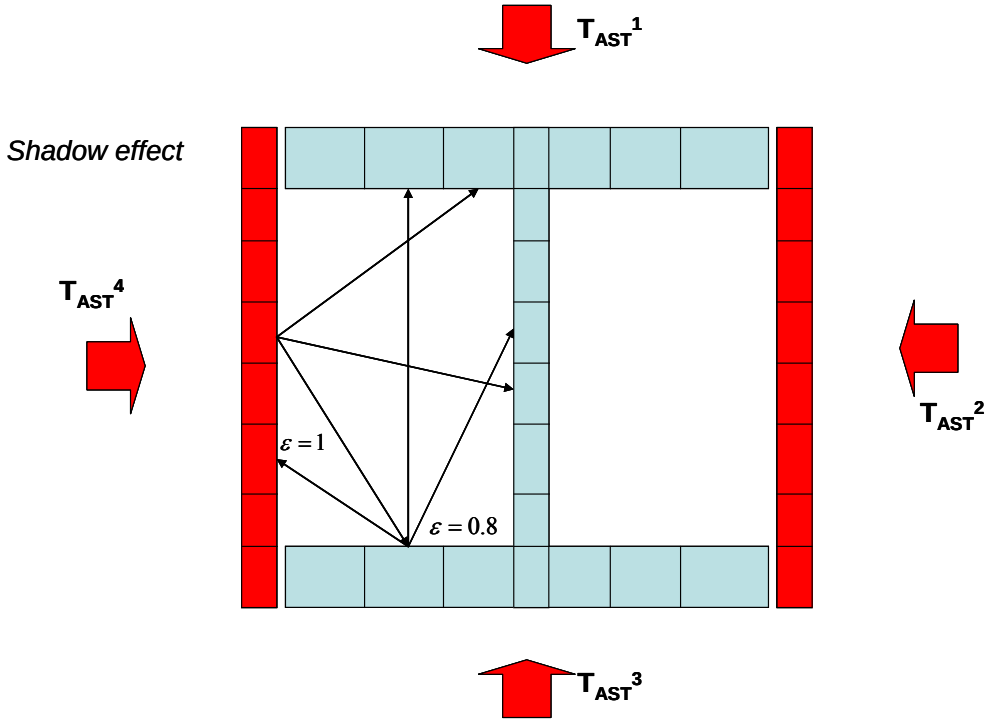

Figure 18 The finite element model of the I-section. The area between the flanges were considered as virtual voids with a virtual thermal boundary between the tips of the flanges.

In these calculation the emissivity of the steel surfaces are assumed equal 0.7 as recommended in Eurocode 3 for fire exposed surfaces. The convection heat transfer coefficient of the outer sides of the webs is assumed equal 25 W/m^{2}K (as recommended in Eurocode 3) and a smaller value of 10 W/m^{2}K at the inner surfaces of the flanges and the web.

7 FDS calculations

Successful predictions of the gas, plate thermometer, adiabatic surface as well as of the steel temperatures has been carried out at NIST [14] with the CFD code FDS. ASTs can be calculated and reported as an post-processing option of FDS.

8 Error estimates

The uncertainties of the reported thermocouple and plate thermometer measurements reported here are deemed to be negligible in comparison to other uncertainties. The main errors of the calculated temperatures shown in Appendix D are due to the high temperature and radiation gradients in the gas phase surrounding the beams. Only one measurement were done on each side of the steel sections and at a distance of 10 cm from the steel surface.

9 Summary and conclusions

Three tests have been carried out, described and analyzed. Gas phase fire temperature have been measured with various types of thermocouples and with plate thermometers. The three types of thermocouples obtained almost the same temperatures while the plate thermometers recorded considerably lower temperature when facing cool surfaces but higher temperature when facing the fire plume.

Adiabatic surface temperatures were obtained by a simple inverse calculation technique based on the plate thermometer recordings only. It was shown that except for the first five minutes, the calculated adiabatic surface temperature were very close to the corresponding plate thermometer recordings even if the fire gas phase temperatures developed very fast.

The temperature of the steel beams were predicted with the finite element code Tasef with the adiabatic surface temperatures as obtained from plate thermometer recordings used as the boundary input data. Given the very challenging scenario with very inhomogeneous thermal conditions and the very simple measurements and the straightforward standard heat transfer model used, the predictions must be considered very accurate. Our experience from these tests and calculations are proof that the concept adiabatic surface temperature and the plate thermometer temperature measurements work very well.

10 References

[1] Van de Leur, P.H.E. and Twilt, L., Fire Resistance Furnace Calibration. TNO-Report 96-CVB-R1323, 1996.
[2] Wickström, U., Heat transfer and temperature calculations based on plate thermometer measurements, Conference proceedings, Fire and materials 2009, San Francisco, 2009.
[3] Mohammed Sultan, personal communication.
[4] Wickström, U., Methods for Predicting Temperature in Fire-Exposed Structures, The SFPE handbook of Fire Protection Engineering, 4th ed., NFPA, Quincy, MA, USA, Chapter 4-9, 2008.
[5] Holman, , J.P., Heat Transfer, 4th ed., McGraw Hill, 1976.
[6] Wickström,U.,Duthinh, D. and McGrattan, K.B., Adiabatic Surface Temperature for Calculating Heat Transfer to Fire Exposed Structures, Interflam 2007.
[7] McGrattan, K.B., Hostikka S., J.E. Floyd, H.R. Baum and R.G. Rehm, Fire Dynamics Simulator (Version 5), Technical Reference Guide, NIST SP 1018-5, National Institute of Standards and Technology, Gaithersburg, Maryland, July 2005.
[8] EN 1991-1-2, Eurocode 1: Actions on structures – Part 1-2: General actions – Actions on structures exposed to fire.
[9] Ingason, H., and Wickström U., *Fire Safety Journal*, **xx**(x)(2006) xxx-yyy
[10] Wickström, U. and Hermodsson, T.
[11] Wickström, U., Calculation of heat transfer to structures exposed to fires - shadow effects, Interflam 2001.
[12] EN 1993-1-2, Eurocode 3: Design of steel structures – part 1-2: General rules – Structural fire design.
[13] Sterner, E. and Wickström, U., TASEF - Temperature Analysis of Structures Exposed to Fire, SP Report 1990:05, Swedish National Testing and Research Institute, Borås, 1990.
[14] Kevin McGrattan et.al., NIST Special Publication 1018-5, Fire Dynamics Simulator (Version 5), Technical Reference Guide, Volume 3: Validation, February 23, 2009, National Institute of Standards and Technology, Gaithersburg, Maryland.

Appendix A – Measured gas phase temperatures

In this annex the temperatures in the gas phase are given as directly measured by thermocouples and plate thermometers.

Notations:
PT = plate thermometer, WT = welded thermocouple, QT = quick tip, and TC = shielded thermocouple.

Numbering of TCs and PTs. The numbering is in the same order as the positons:
Measuring station A, position 1 – 4: number 1 – 4
Measuring station B, position 1 – 4: number 5 - 8
Measuring station C, position 1 – 4: number 9 - 12

Test 1 Hollow square beam, burner in the corner

The measured temperatures at measuring station A are given in four diagrams, one for each position, see Figure 19 to Figure 22.

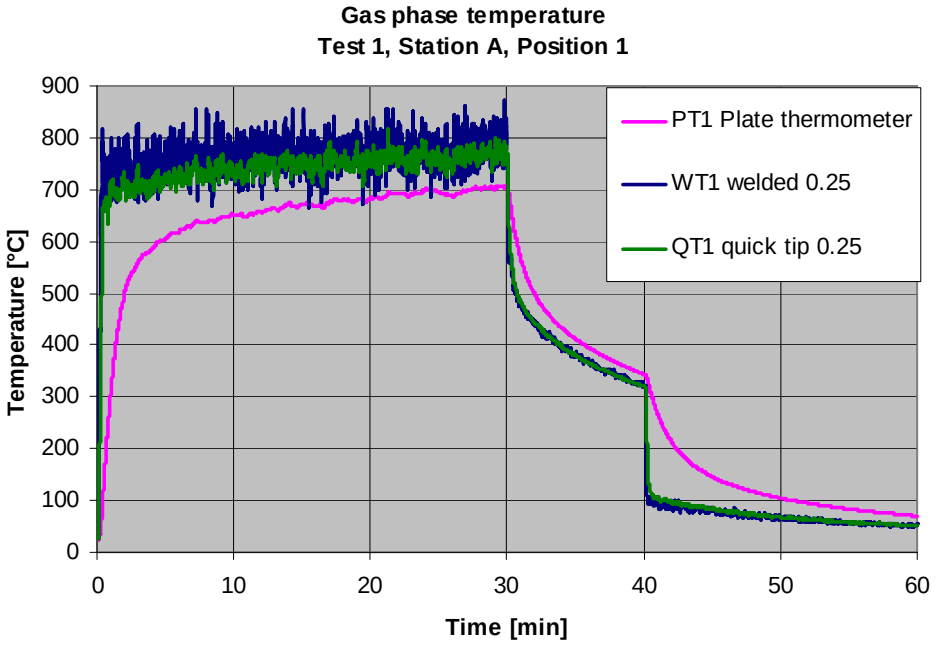

Figure 19 Plate thermometer (PT) and gas phase thermocouple (welded WT and quicktip QT) measurements above the steel beam. Test 1, station A, position 1.

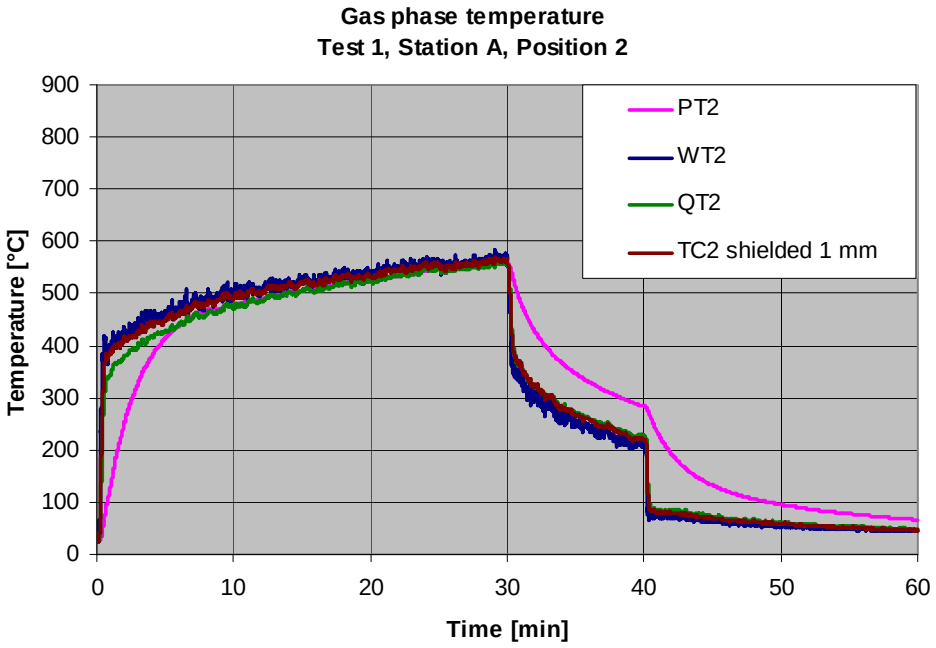

Figure 20 **Plate thermometer (PT) and gas phase thermocouple (welded WT, quicktip QT and shielded TC) measurements opposite burner side of the beam. Test 1, station A, position 2.**

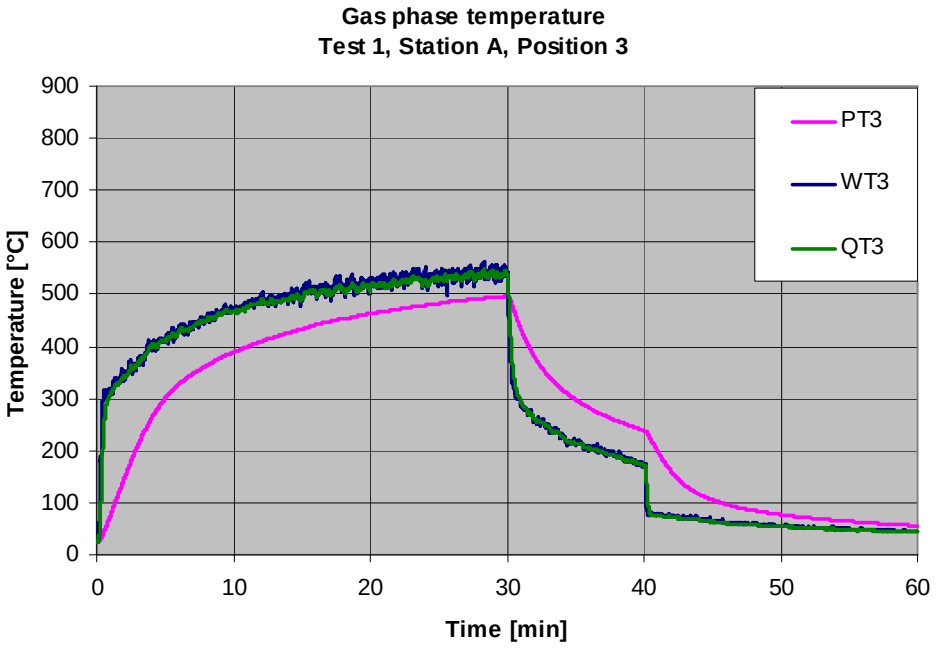

Figure 21 **Plate thermometer (PT) and gas phase thermocouple (welded WT and quicktip QT) measurements below the beam. Test 1, station A, position 3.**

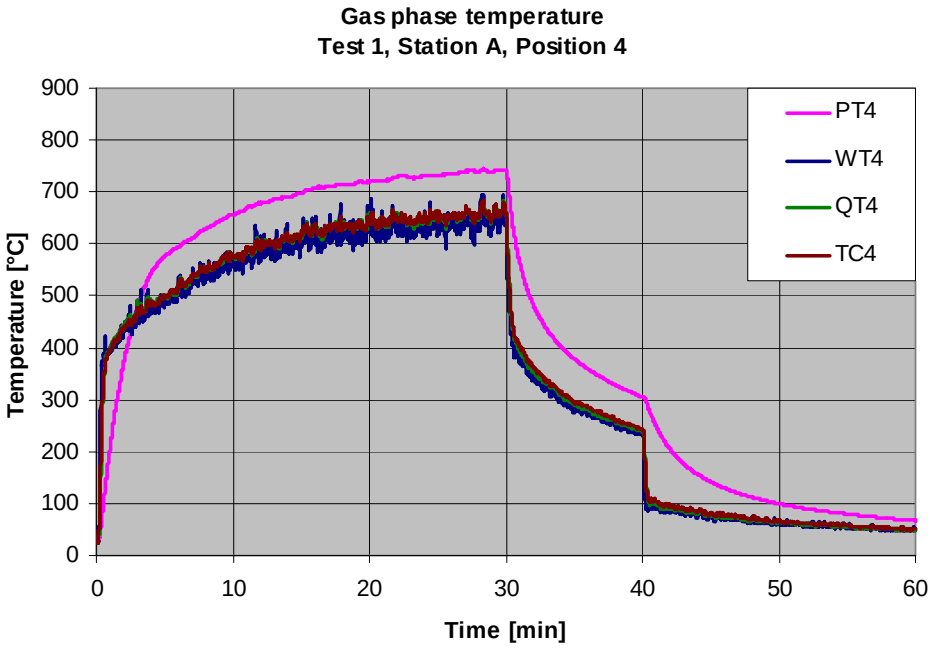

Figure 22 **Plate thermometer (PT) and gas phase thermocouple (welded WT, quicktip QT and shielded TC) measurements on theburner side of the steel beam. Test 1, station A, position 4.**

All the temperatures at measuring station B and C are given in Figure 23 and Figure 24, respectively.

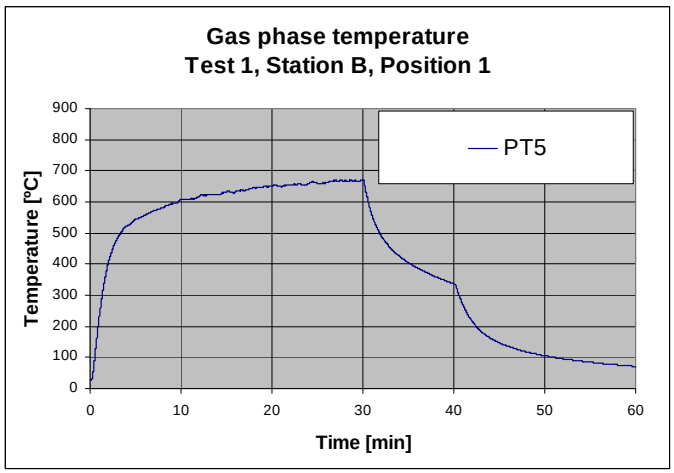

a) Position 1

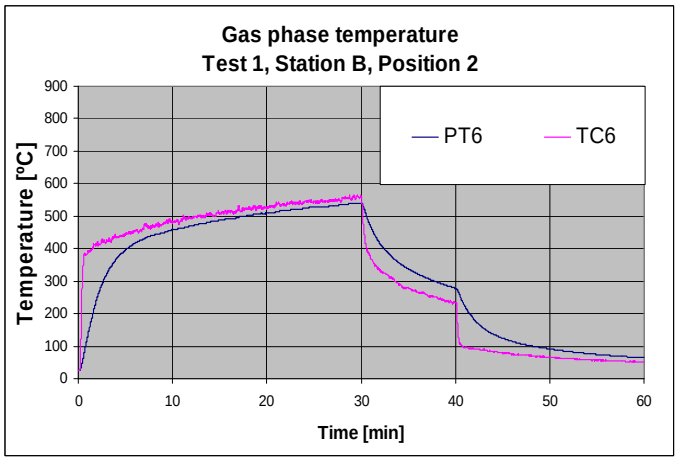

b) Position 2

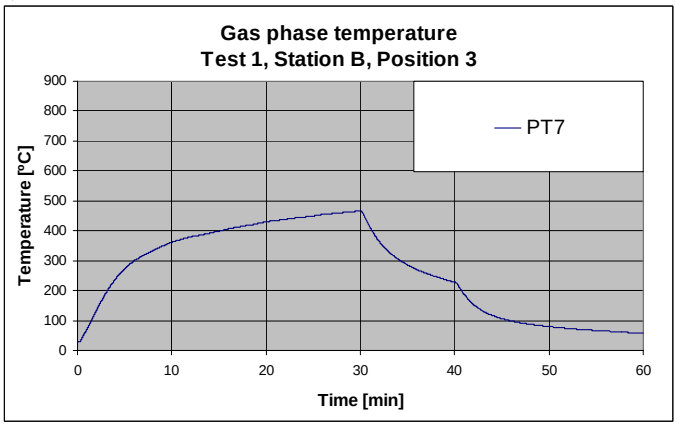

c) Position 3

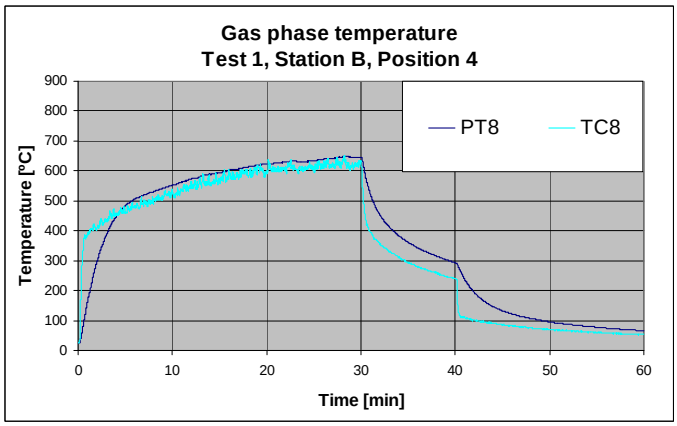

d) Position 4

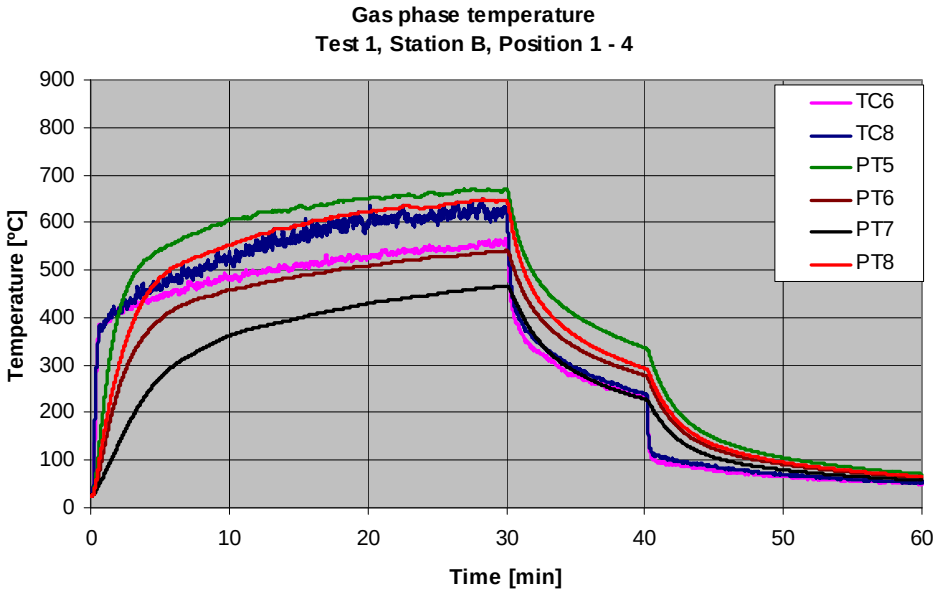

Summary, Positions 1 – 4.

Figure 23 Gas temperature and plate thermometer measurements at Measuring Station B, Position 1 – 4.

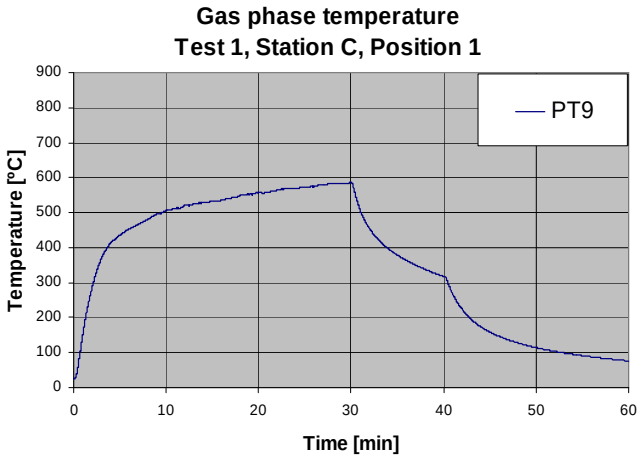

a) Position 1

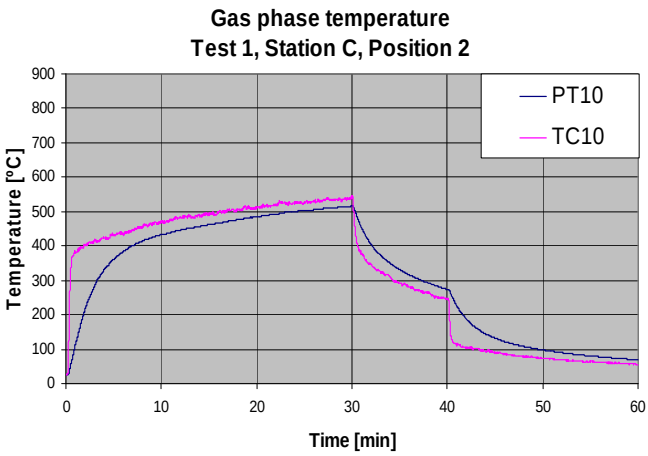

b) Position 2

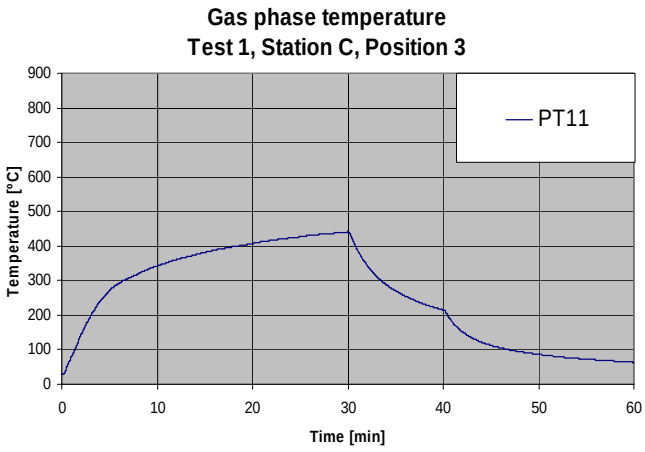

c) Position 3

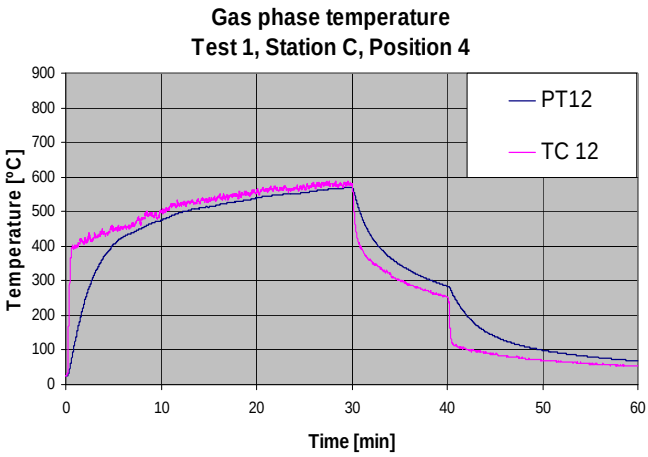

d) Position 4

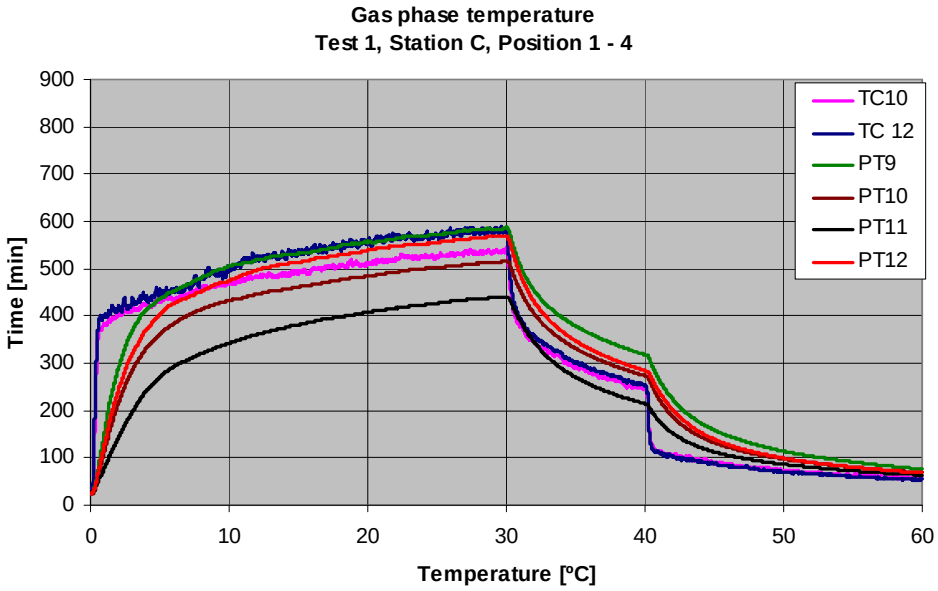

e)

Summary, Positions 1 – 4

Figure 24 Gas temperature and plate thermometer measurements at Measuring Station C, Position 1 – 4.

Test 2 I-beam, burner in the corner

The measured temperatures of Test 2 at measuring station A are given in four diagrams, one for each position, in Figure 25.

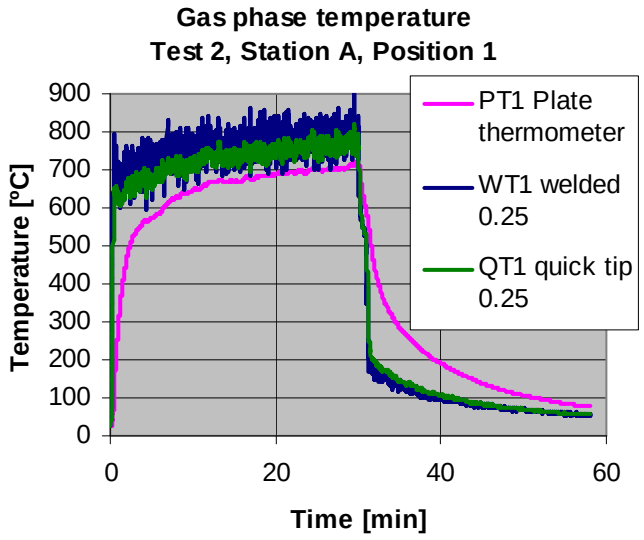

a) Position 1

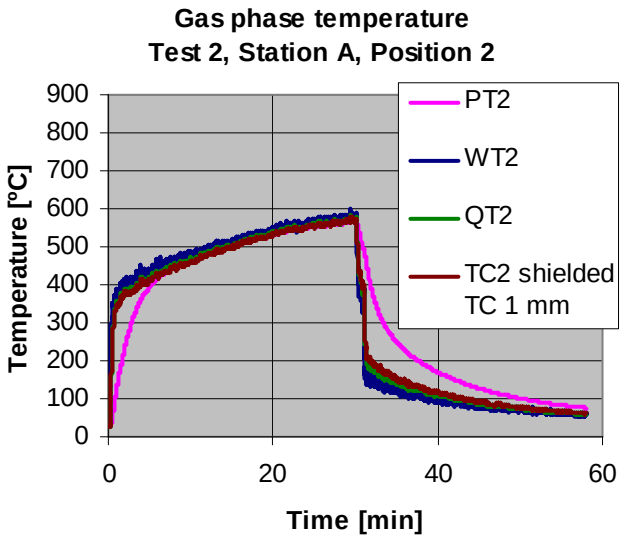

b) Position 2

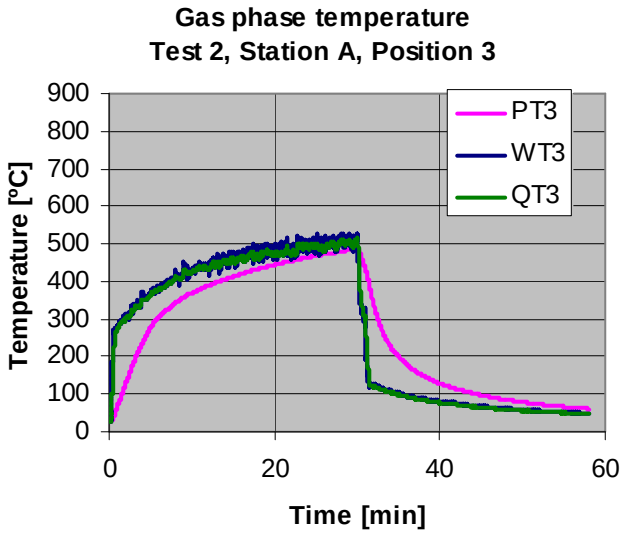

c) Position 3

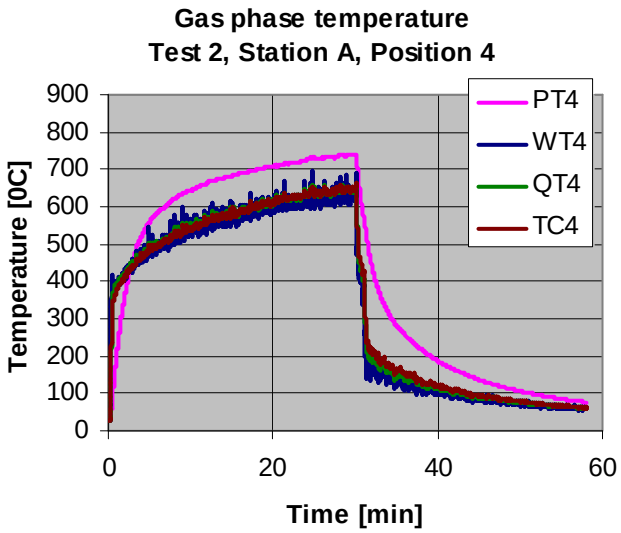

d) Position 4

Figure 25 Plate thermometer and gas phase thermocouple measurements. Test 2, station A, positions 1 - 4.

All the temperatures at measuring station B and C are given in Figure 26 and Figure 27, respectively.

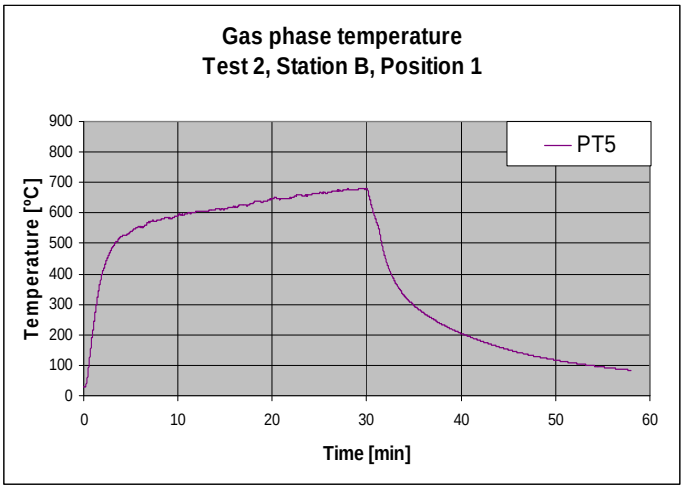

a) Position 1

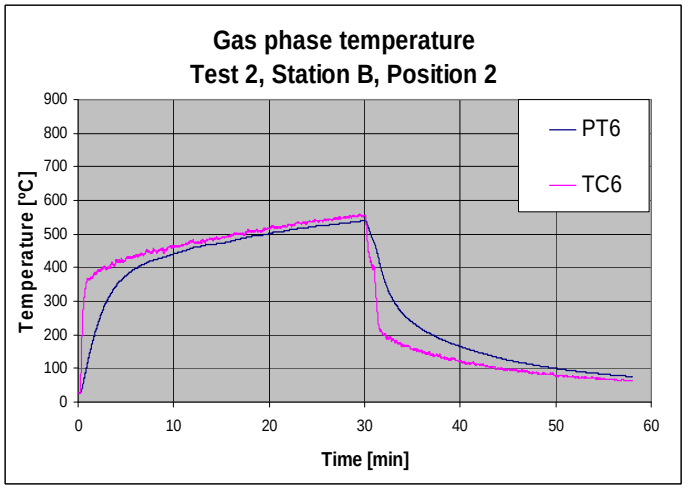

b) Position 2

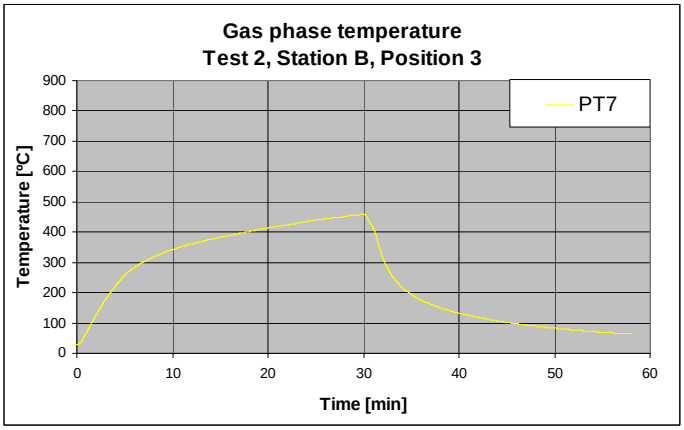

c) Position 3

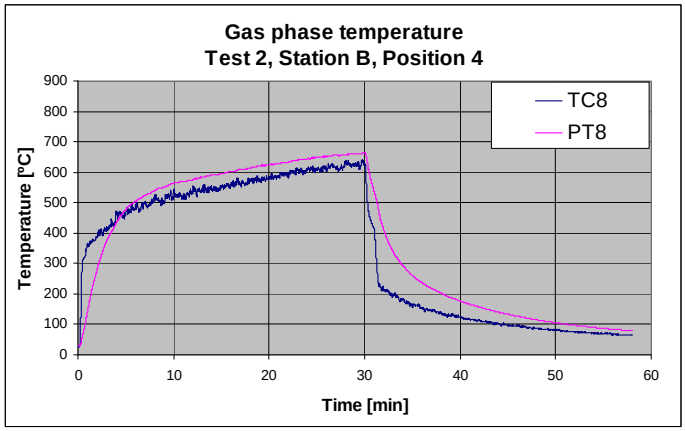

d) Position 4

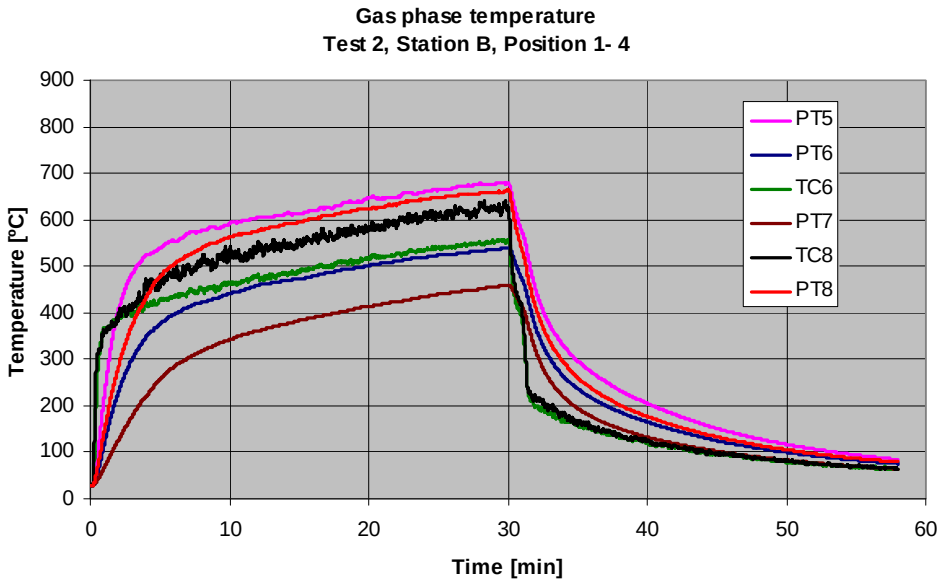

e) Summary, Positions 1 -4.

Figure 26 Gas temperature and plate thermometer measurements at Measuring Station B, Position 1 – 4.

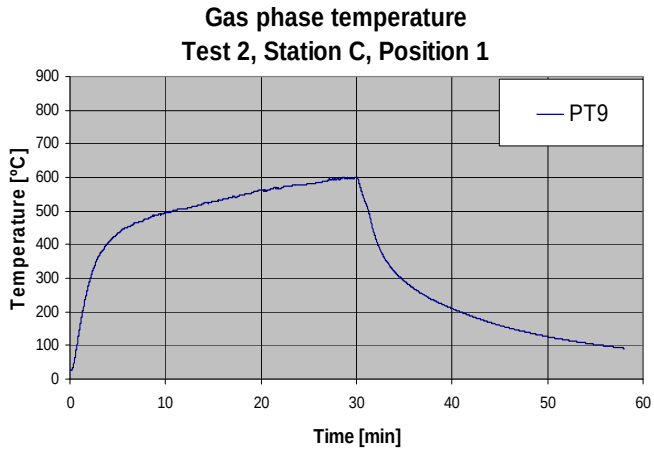

a) Position 1

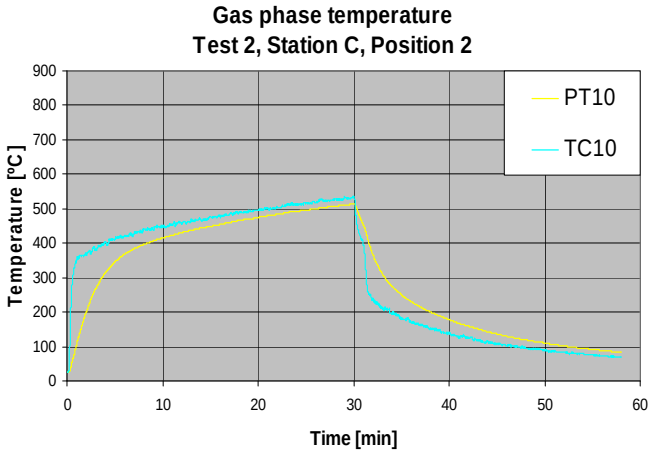

b) Position 2

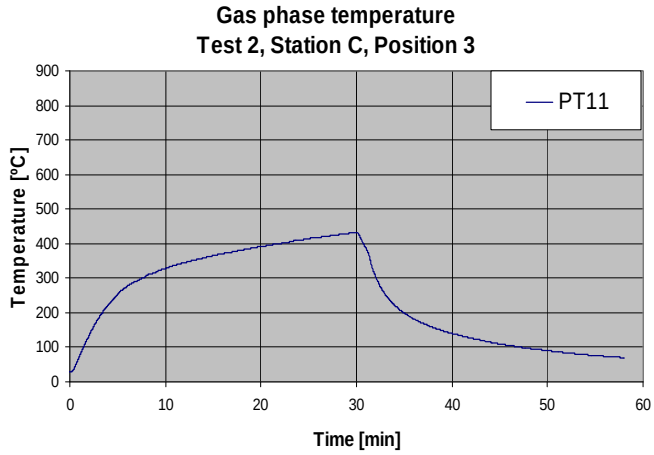

c) Position 3

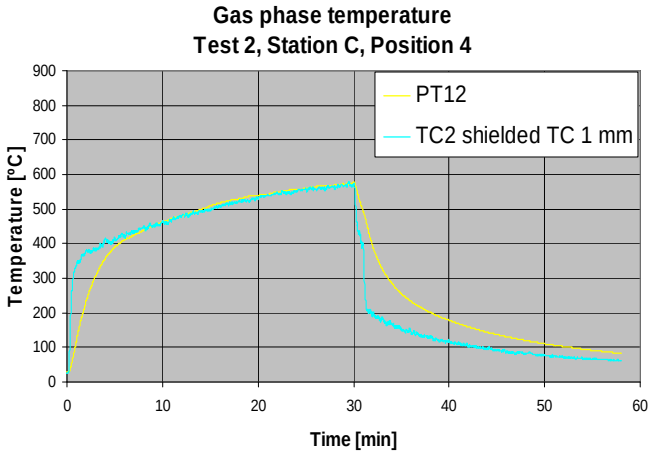

d) Position 4

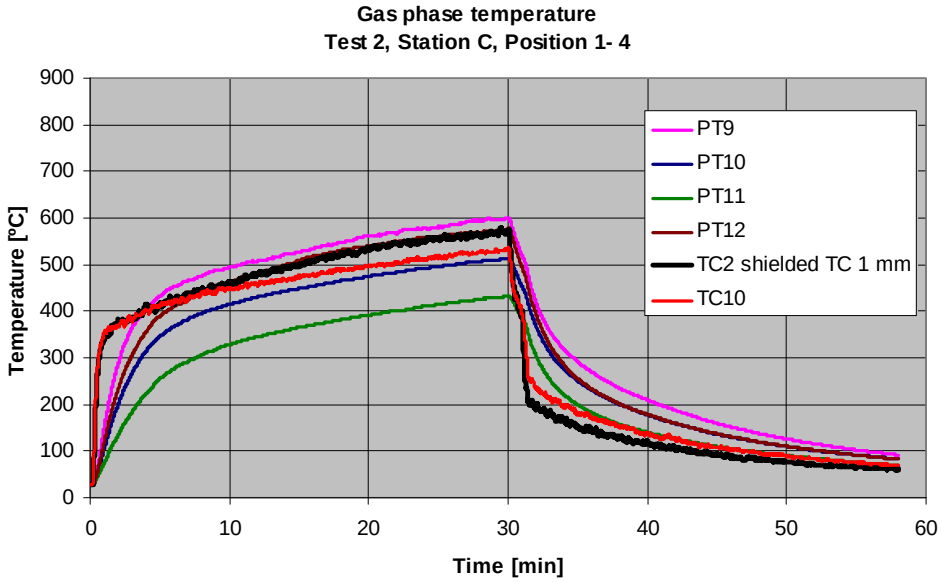

e) Summary, Positions 1 - 4.

Figure 27 Gas temperature and plate thermometer measurements at Measuring Station C, Position 1 – 4.

Test 3 I-beam, burner in the corner

The measured temperatures of Test 3 at measuring station A are given in four diagrams, one for each position, in Figure 28.

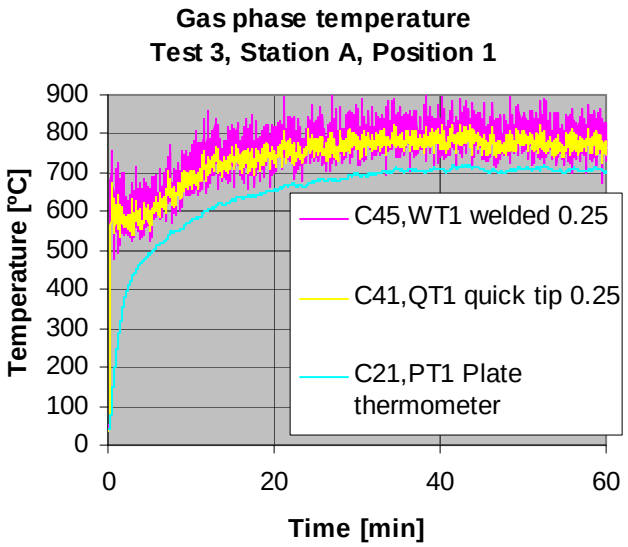

Position 1

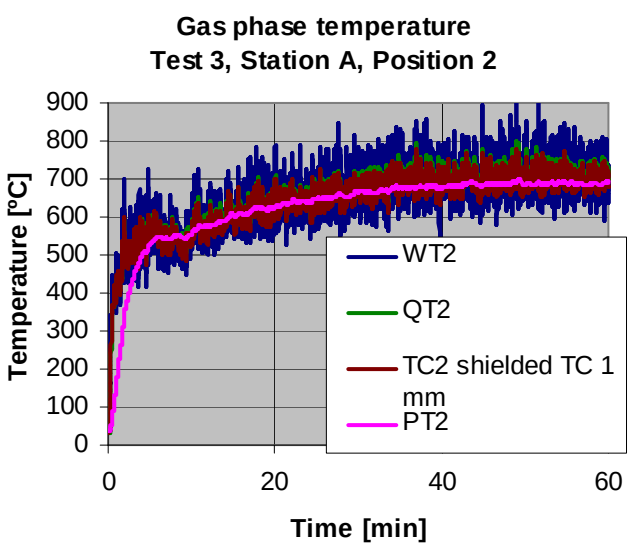

Position 2

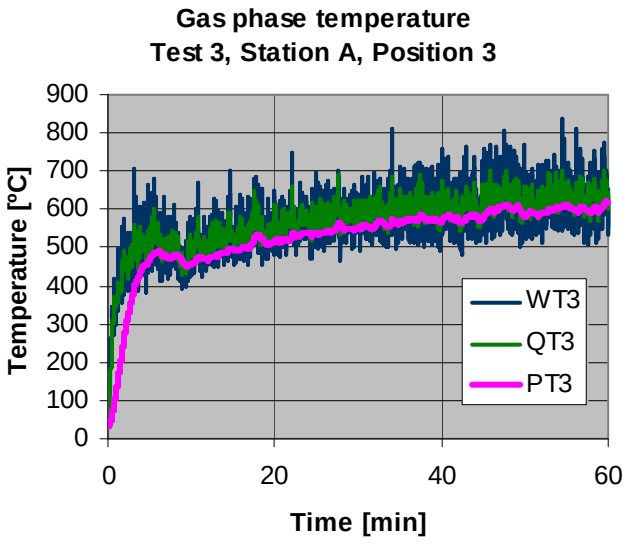

Position 3

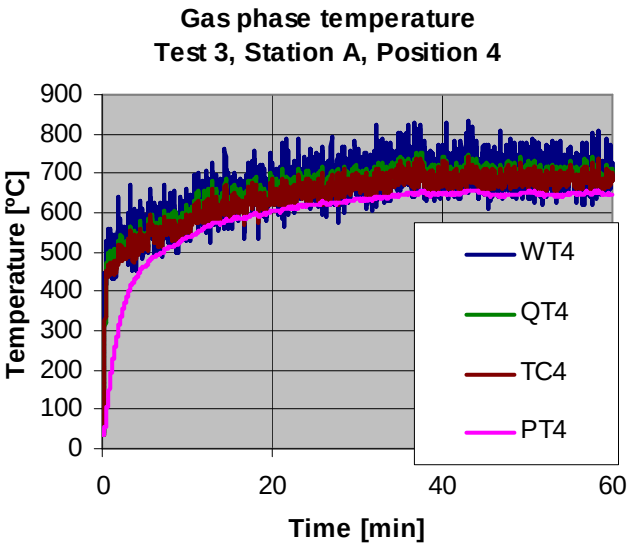

Position 4

Figure 28 Gas temperature and plate thermometer measurements at Measuring Station A, Position 1 - 4.

All the temperatures at measuring station B and C are given in Figure 29 and Figure 30, respectively.

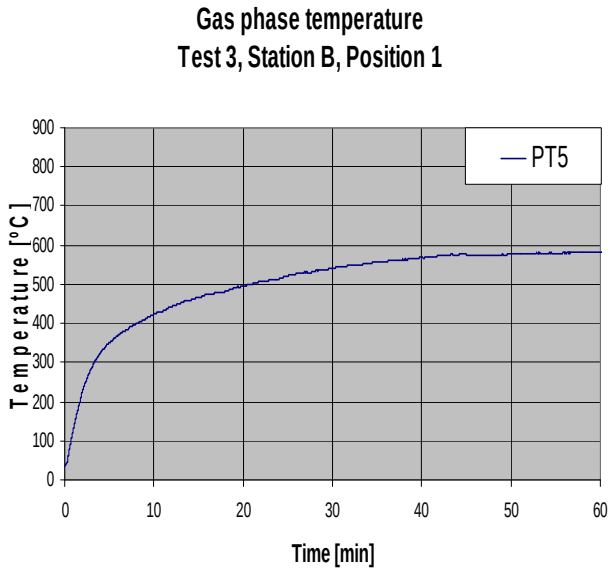

a) Position 1

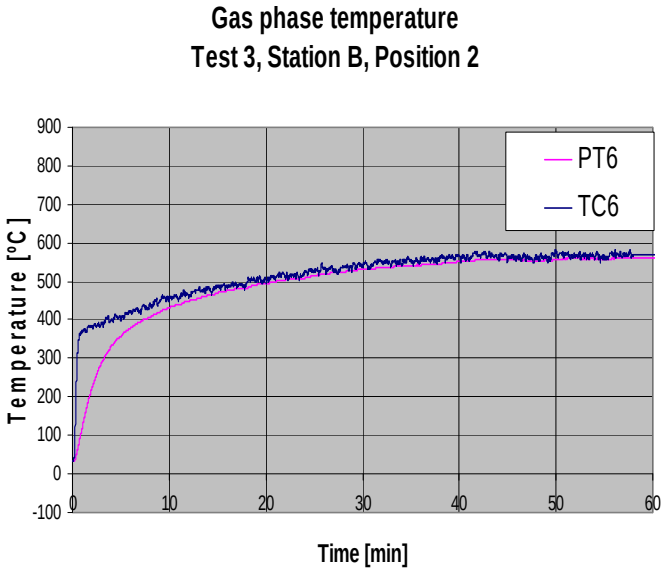

b) Position 2

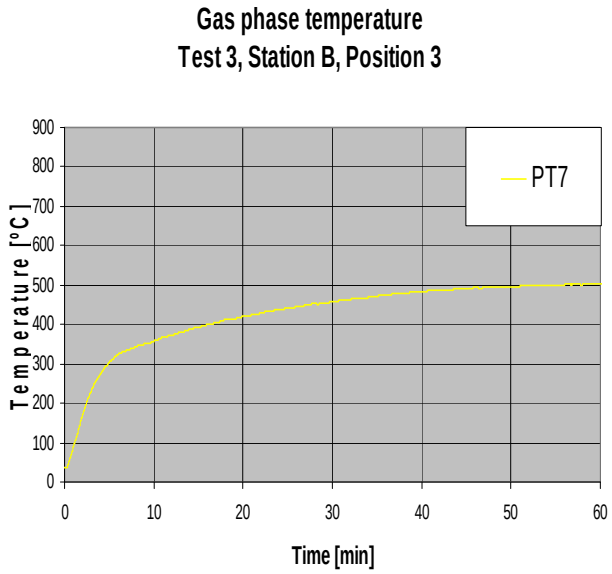

c) Position 3

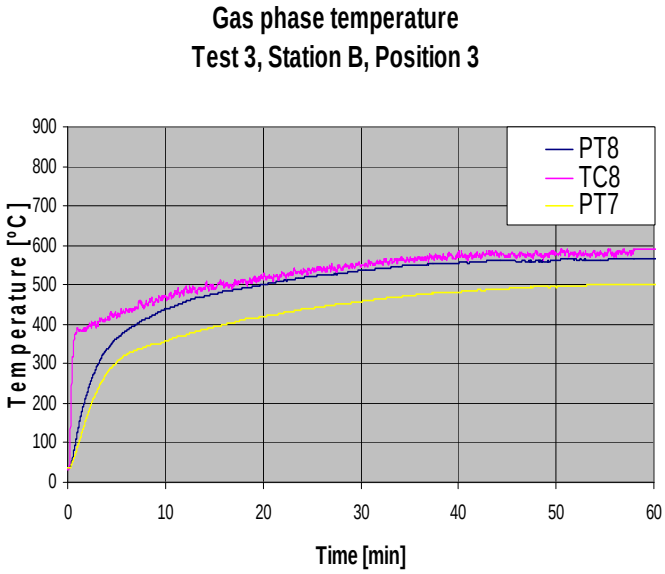

d) Position 4

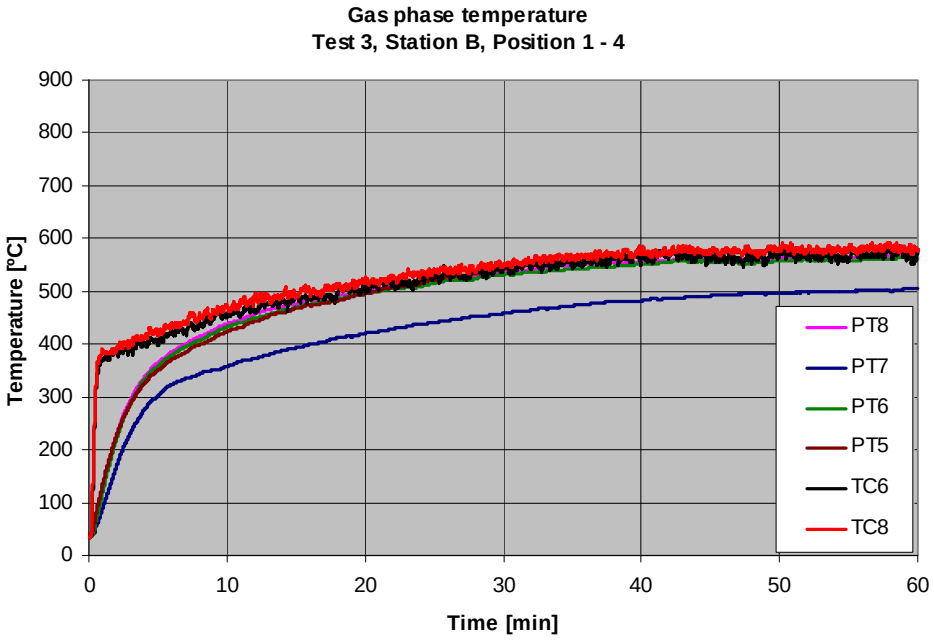

e) Summary, Positions 1 - 4.

Figure 29 **Gas temperature and plate thermometer measurements at Measuring Station B, Position 1 -4.**

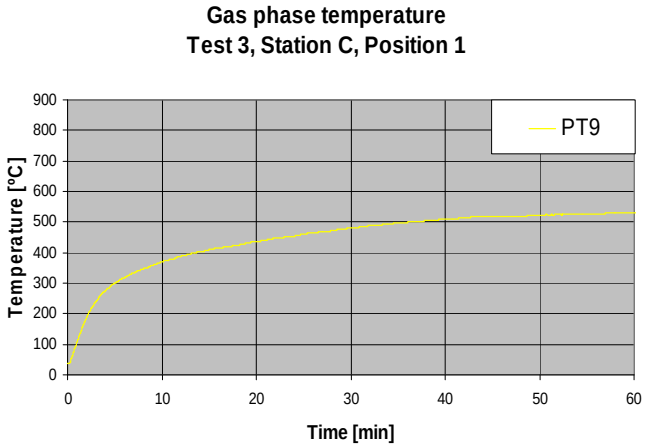

a) Position 1

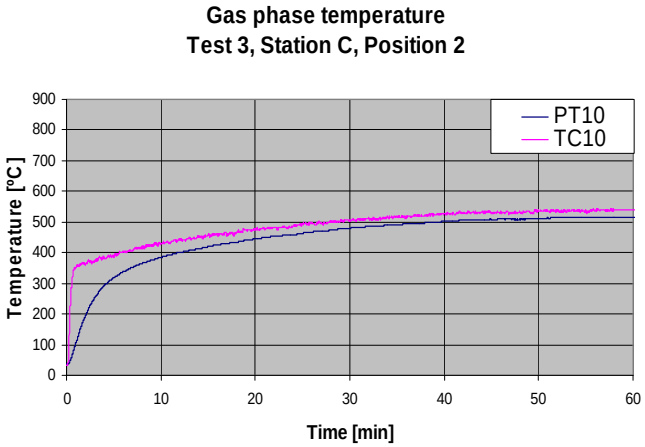

b) Position 2

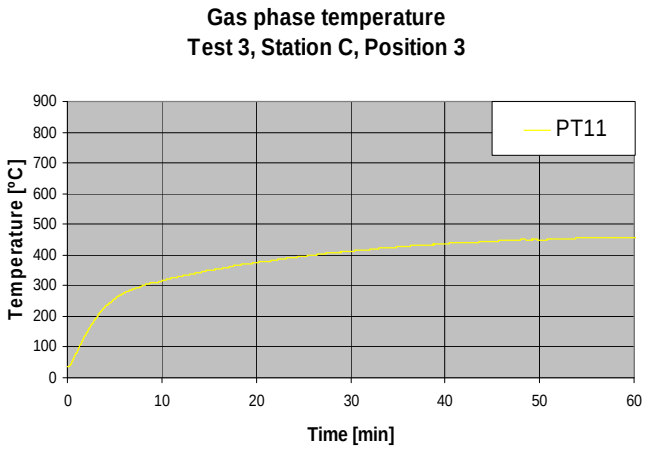

c) Position 3

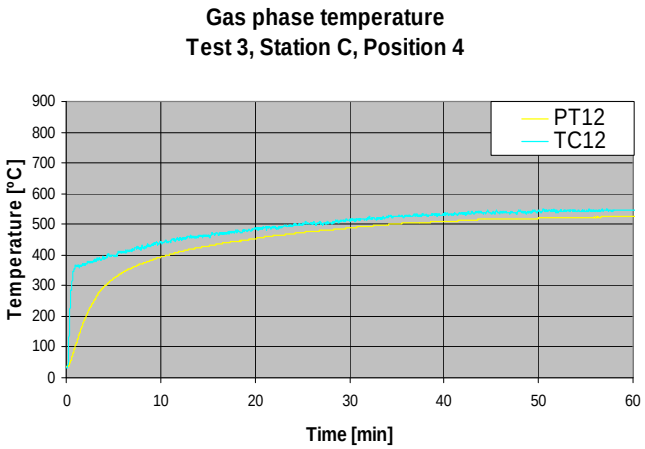

d) Position 4

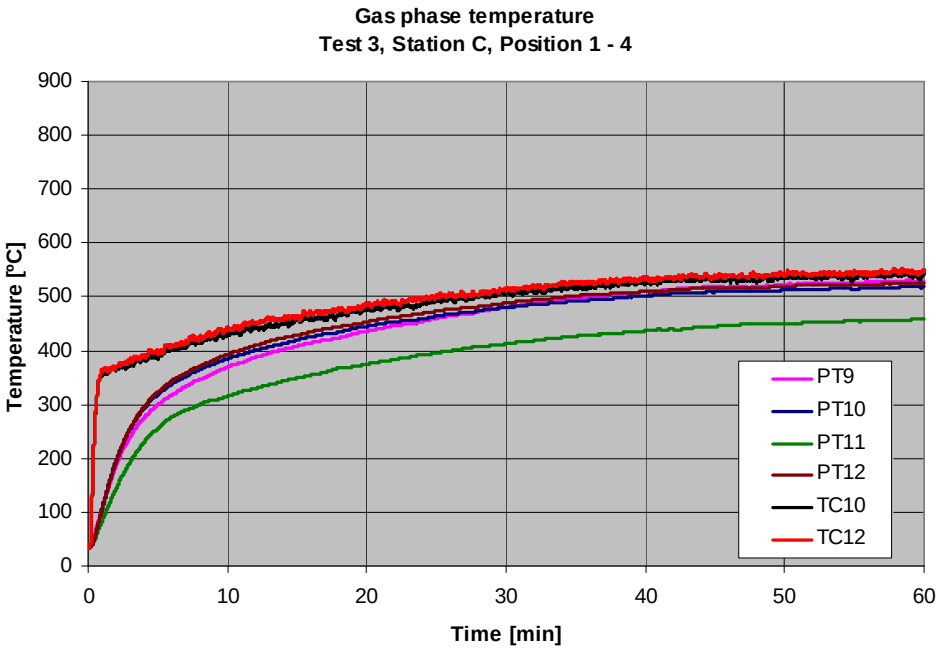

e) Summary, Positions 1 - 4.

Figure 30 Gas temperature and plate thermometer measurements at Measuring Station C

Appendix B – Measured steel temperatures

In this annex the temperatures in the steel are given as directly measured by thermocouples.

Numbering of TCs. The first number in the diagram legend C1 etc. is the internal measuring channel identification. The next indicates position, see Figure 10.

Test 1 Hollow square beam, burner in the corner

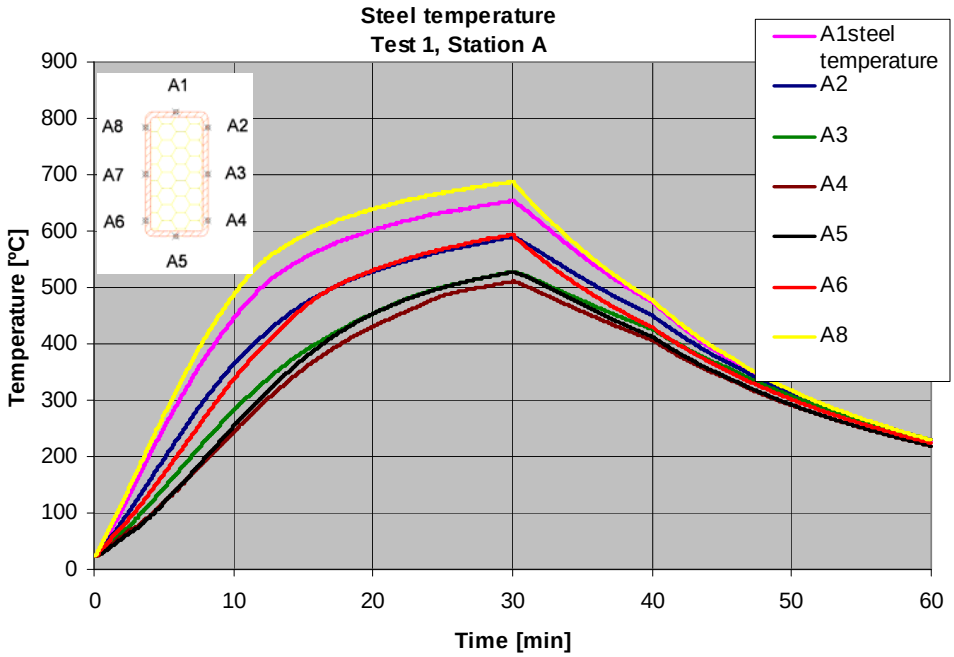

Figure 31 Steel temperatures at Measuring Station A. Placement of steel thermocouples, see Figure 10.

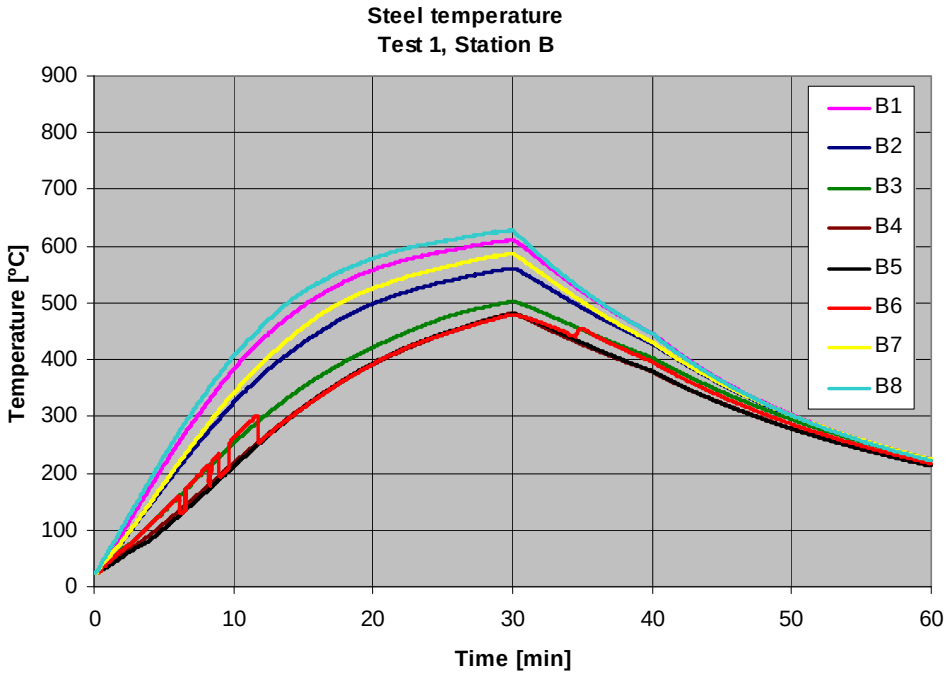

Figure 32 **Steel temperatures at Measuring Station B. Placement of steel thermocouples, see Figure 10.**

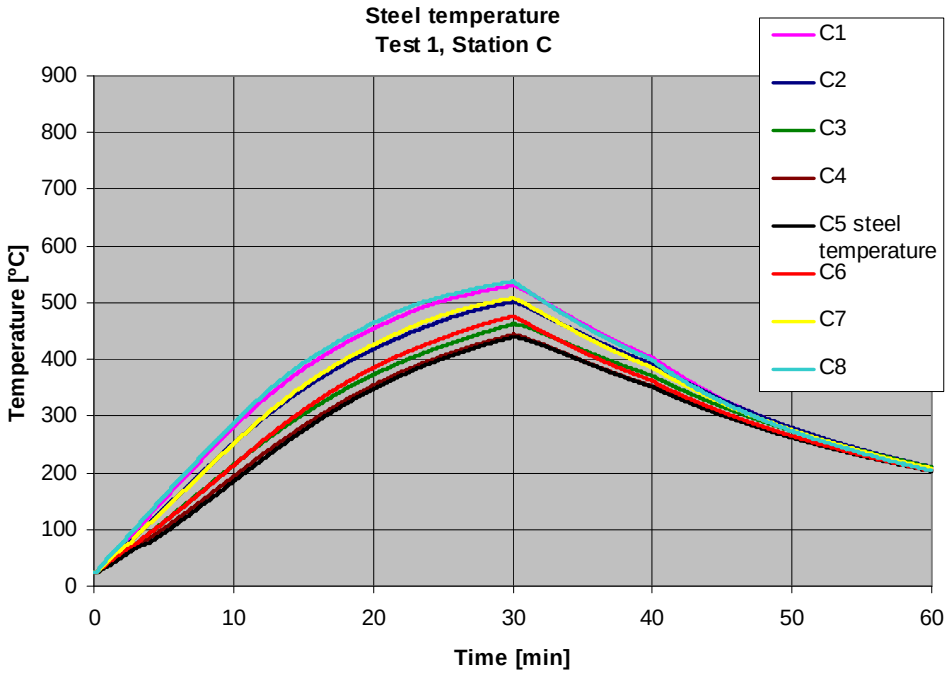

Figure 33 **Steel temperatures at Measuring Station C. Placement of steel thermocouples, see Figure 10.**

Test 2 I-beam, burner in the corner

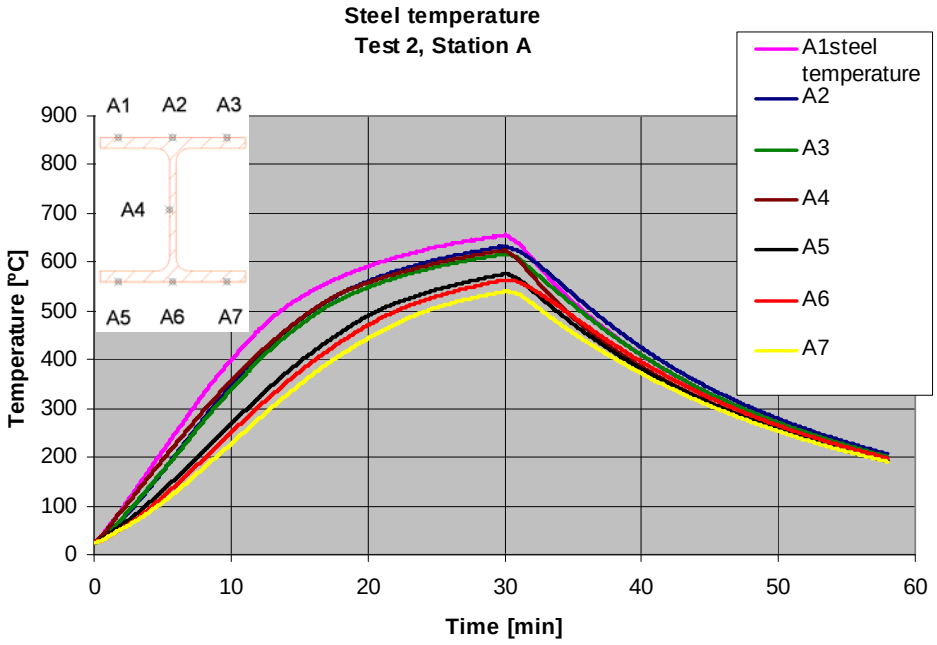

Figure 34 **Steel temperatures at Measuring Station A. Placement of steel thermocouples, see Figure 10.**

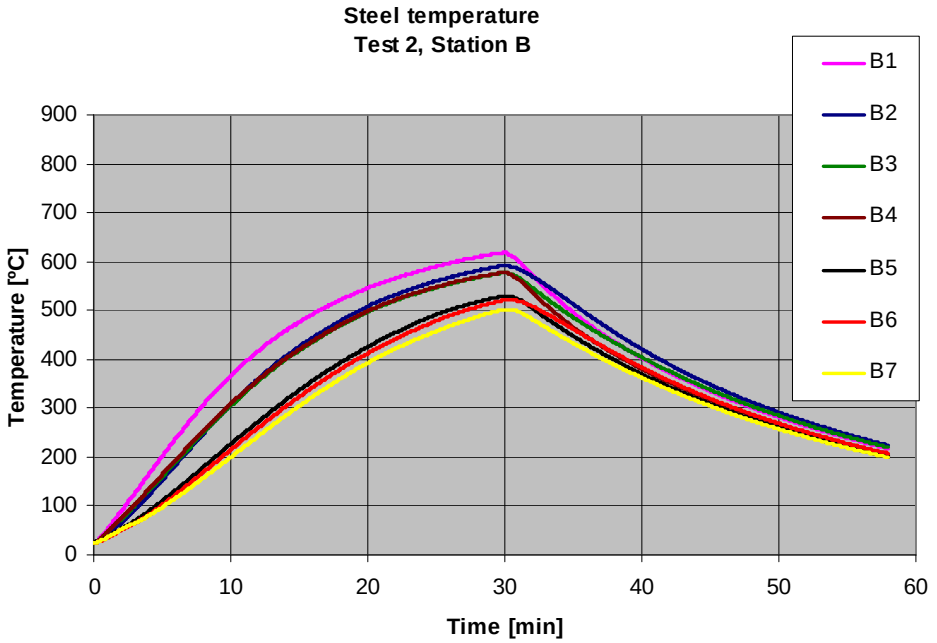

Figure 35 **Steel temperatures at Measuring Station B. Placement of steel thermocouples, see Figure 10.**

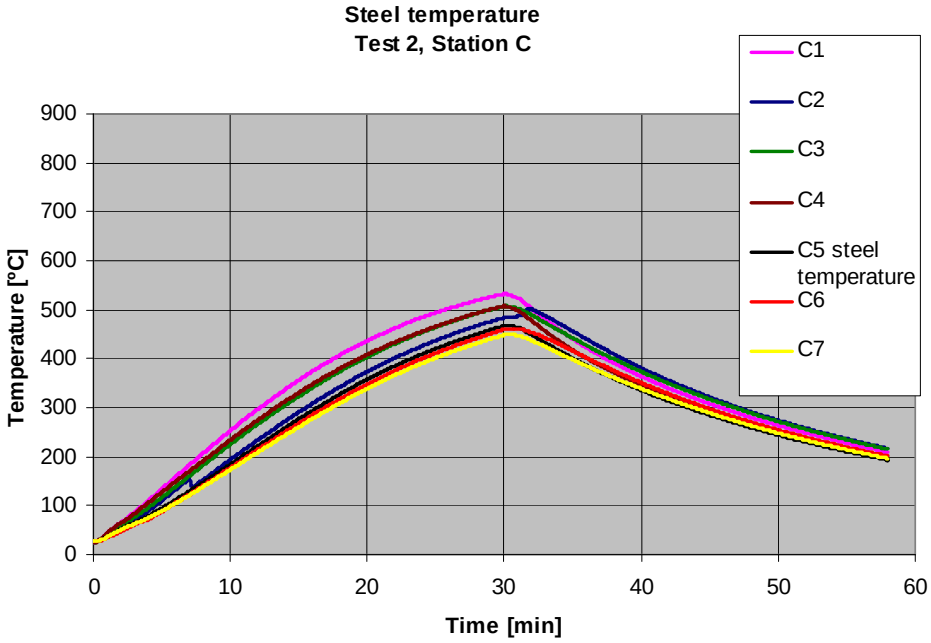

Figure 36 **Steel temperatures at Measuring Station C. Placement of steel thermocouples, see Figure 10.**

Test 3 I-beam, burner in the corner

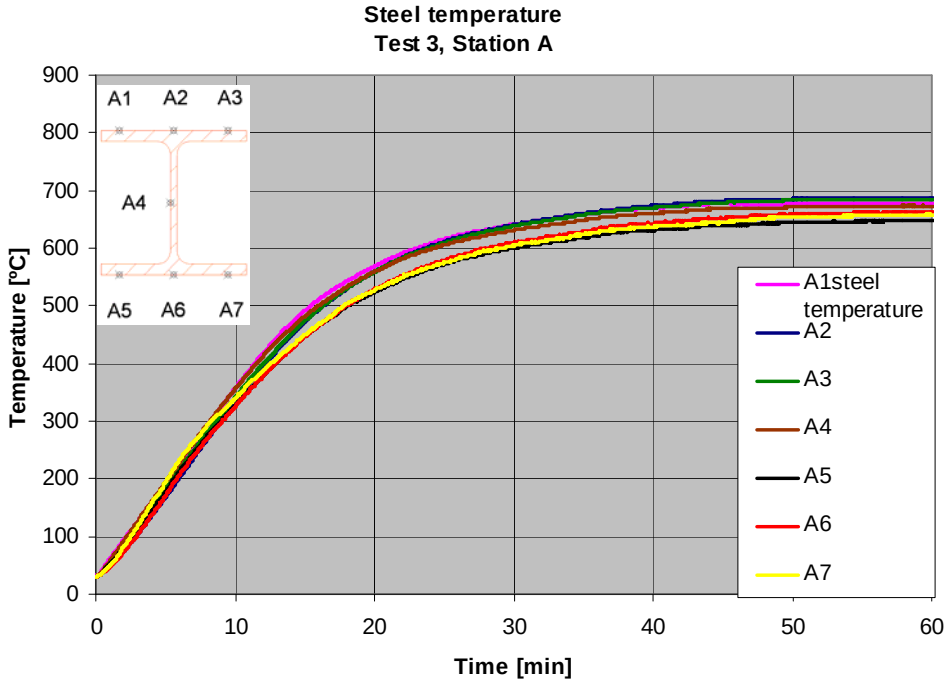

Figure 37 **Steel temperatures at Measuring Station A. Placement of steel thermocouples, see Figure 10.**

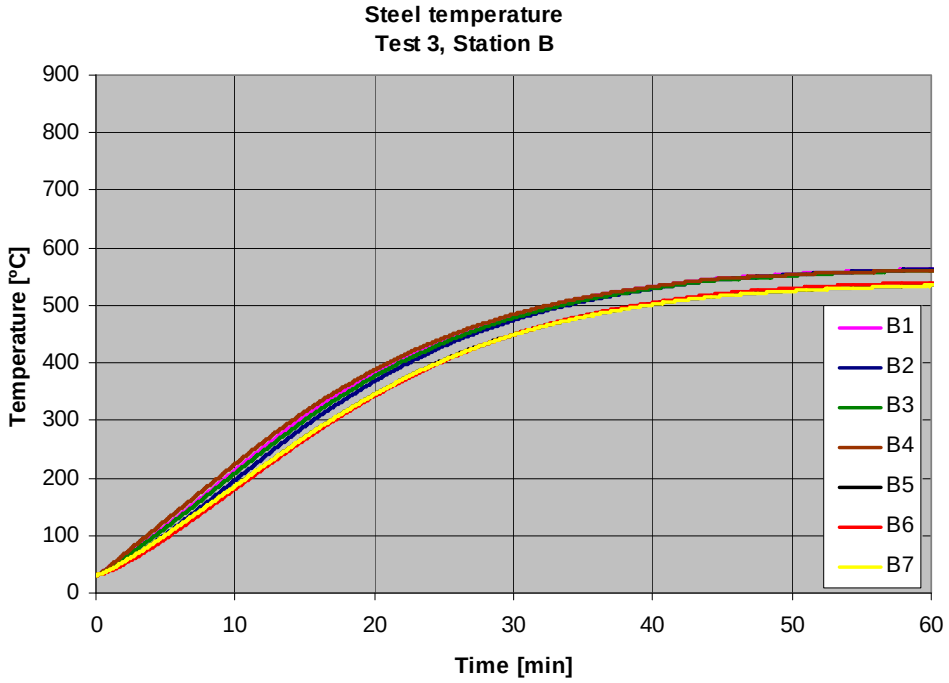

Figure 38 **Steel temperatures at Measuring Station B. Placement of steel thermocouples, see Figure 10.**

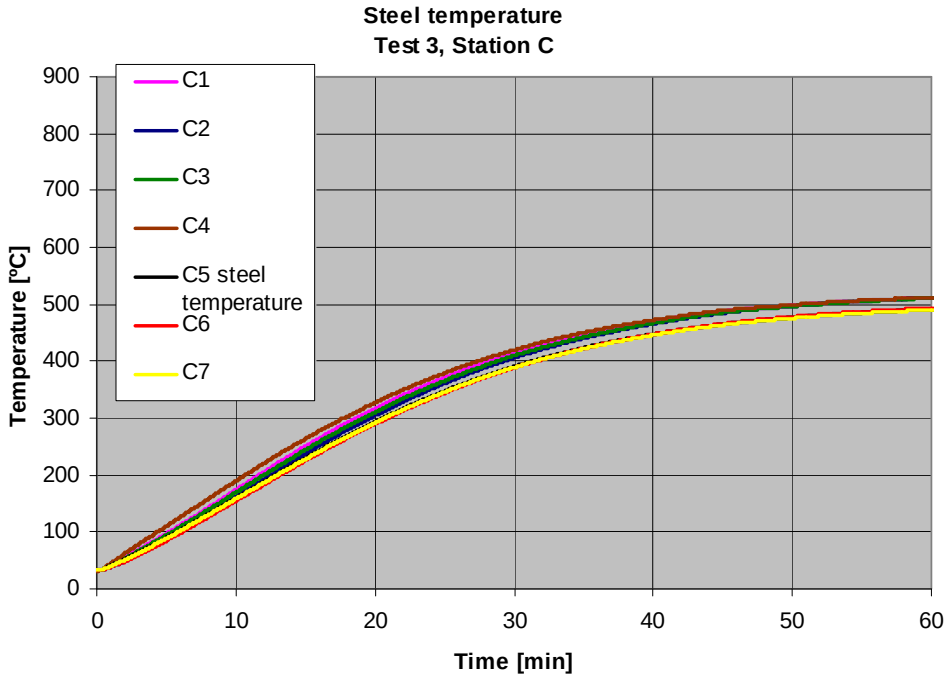

Figure 39 **Steel temperatures at Measuring Station C. Placement of steel thermocouples, see Figure 10.**

Appendix C - Calculated adiabatic surface temperatures

The graphs of the adiabatic surface temperatures are based on the corresponding plate thermometer recordings. Calculations are carried out according to section 2.3.1 assuming the emissivity $\varepsilon = 0.9$ and the convection heat transfer coefficient $h = 20$ W/m^{2}K. Assumptions of slightly different values would only marginally change the calculated ASTs.

Test 1 Hollow square beam, burner in the corner

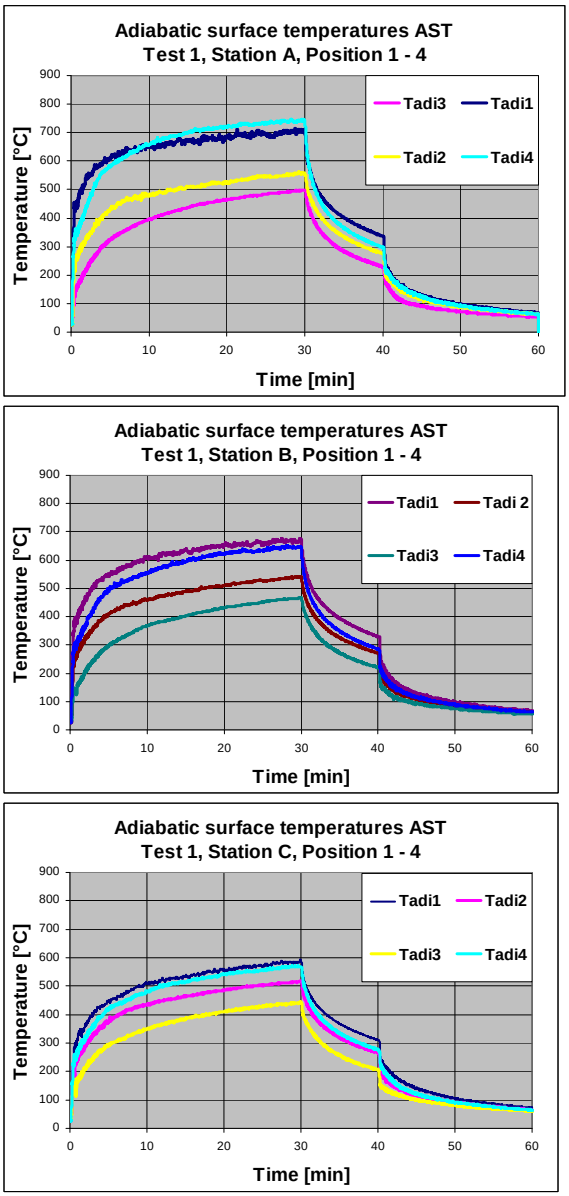

Figure 40 **Adiabatic surface temperature derived from measured PT temperatures. Test 1, stations A - C, postions 1 - 4.**

Test 2 I-beam, burner in the corner

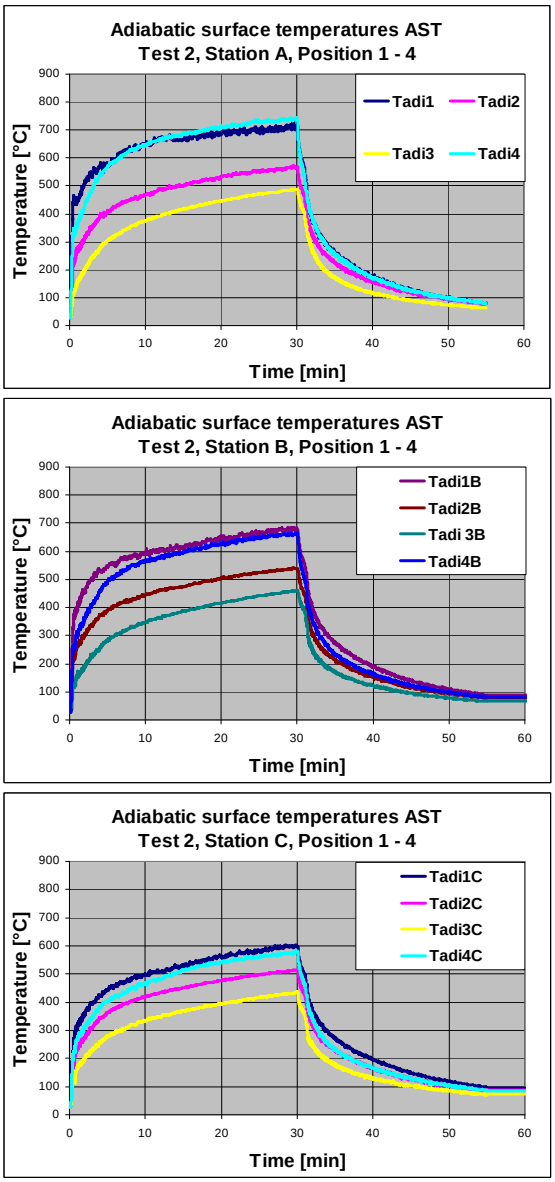

Figure 41 **Adiabatic surface temperature derived from measured PT temperatures. Test 2, stations A - C, postions 1 - 4.**

Test 3 I-beam, burner in the centre

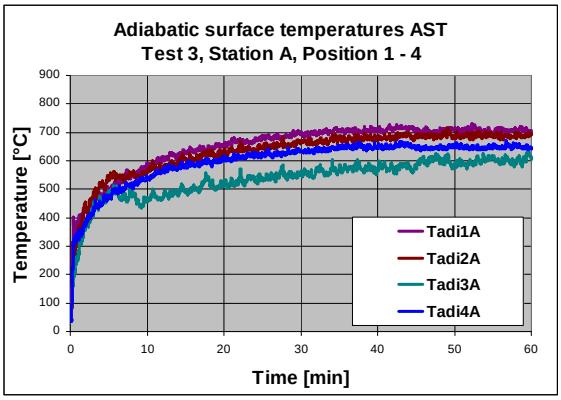

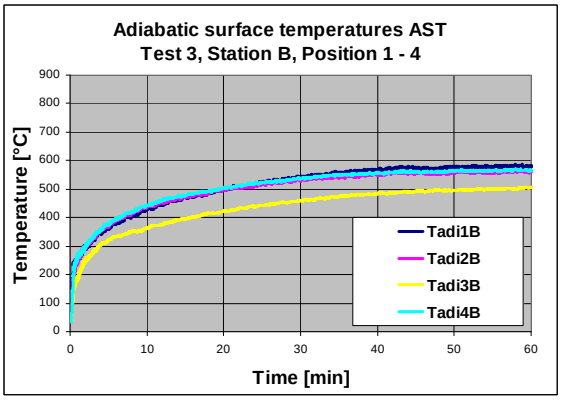

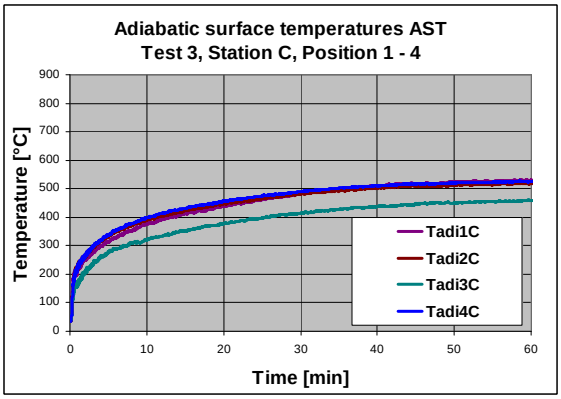

Figure 42 **Adiabatic surface temperature derived from measured PT temperatures. Test 3, stations A - C, postions 1 - 4.**

Appendix D – Comparisons of measured and calculated steel temperatures

The steel temperatures are calculated with the computer code Tasef [13]. The thermal properties of steel assumed in the calculations are as recommended in Eurocode 3 [12]. The boundary conditions are the four adiabatic temperatures at the corresponding section (measuring station) as given in Appendix C - Calculated adiabatic surface temperatures . The heat flux at the boundaries is calculated according to Eq. 15 assuming the steel surface emissivity ε = 0.7 as recommended in Eurocode 3 [12] and the convection heat transfer coefficient h = 25 W/m^2 except in the virtual voids between the flanges and the web of the I-beam sections where the heat transfer coefficient is assumed lower, i.e. h = 10 W/m^2.

Generally for the graphs the full lines are measured and dashed lines are calculated.

Test 1 Hollow square beam, burner in the corner

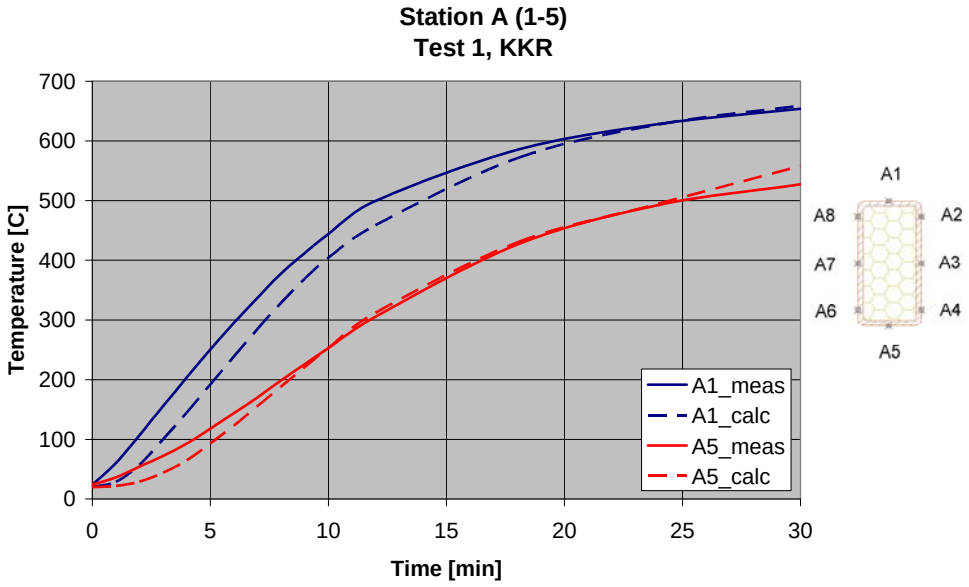

a) Upper and lower sides

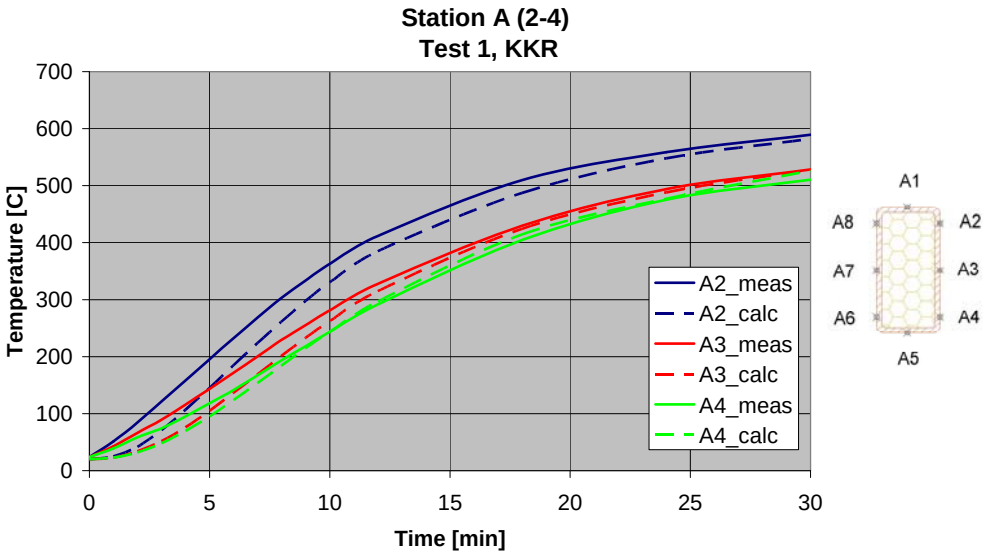

b) Unexposed side

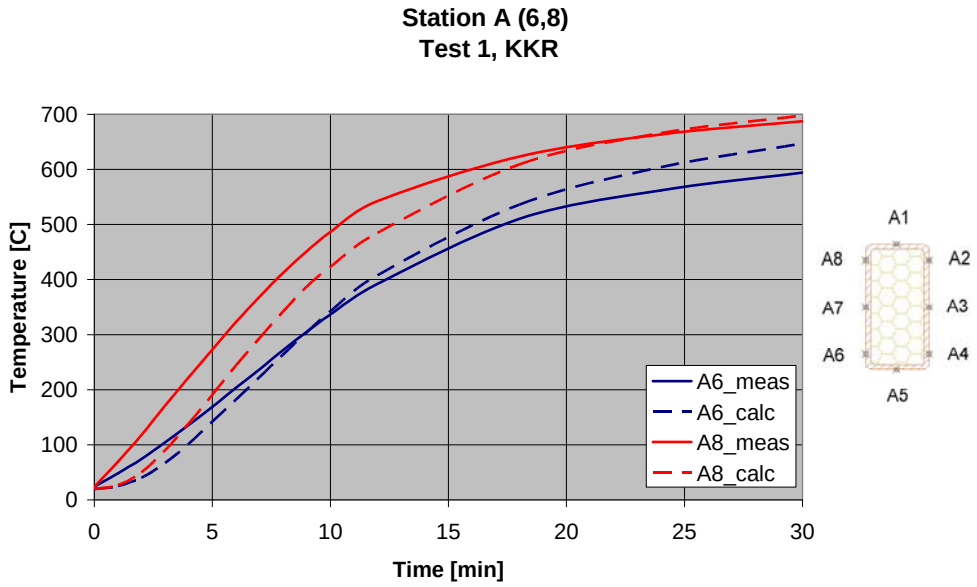

c) Burner side (TC A7 out of order)

Figure 43 Measuring station A: Meausured steel temperature and calculated steel temperature at the corresponding positions as a function on time.

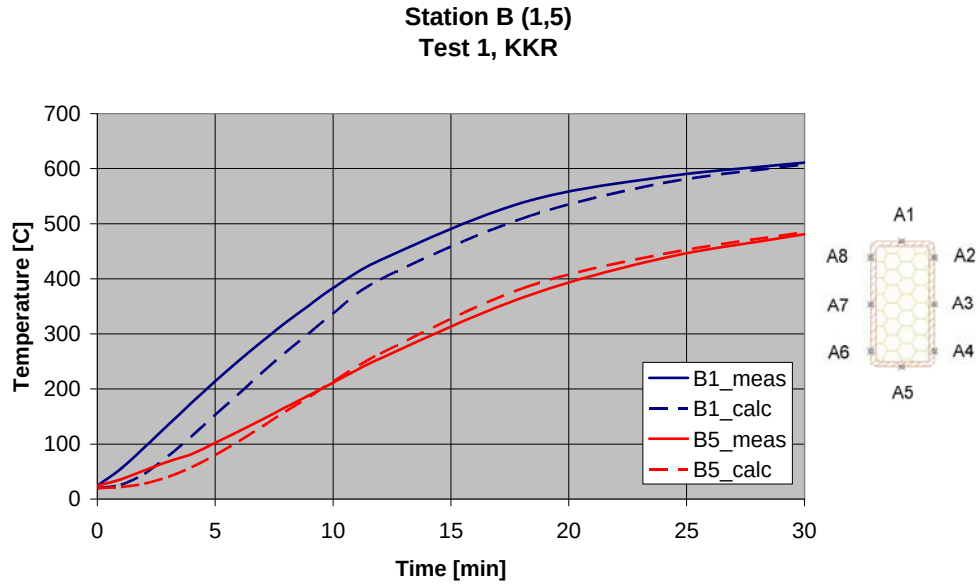

a) Upper and lower sides

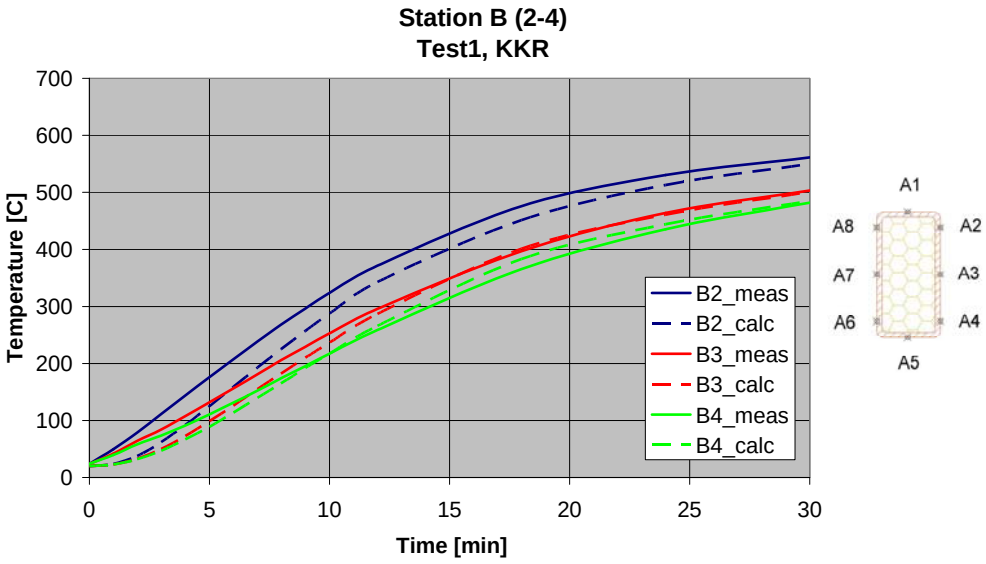

b) Unexposed side

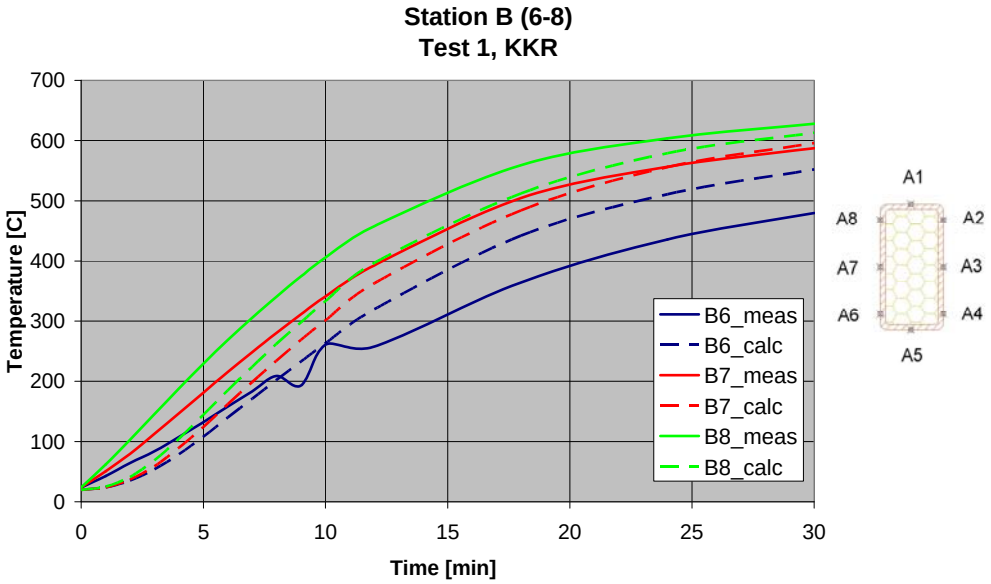

c) Burner side

Figure 44 Measuring station B: Meausured steel temperature and calculated steel temperature at the corresponding positions as a function of time.

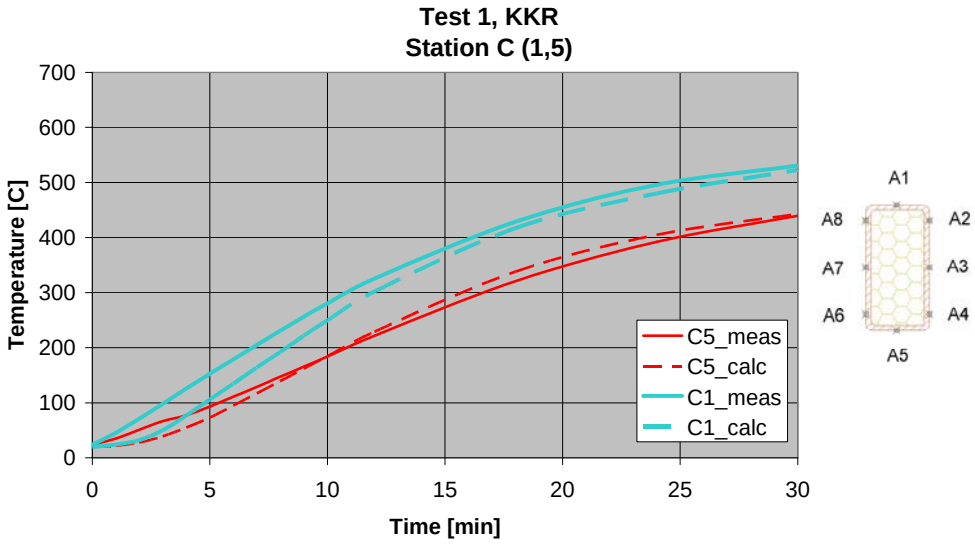

a) Upper and lower sides

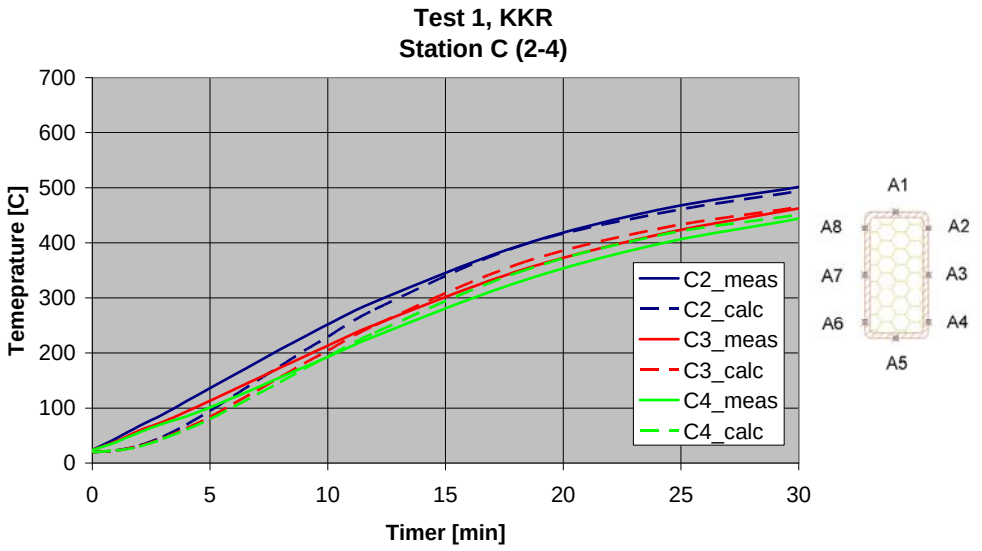

b) Unexposed side

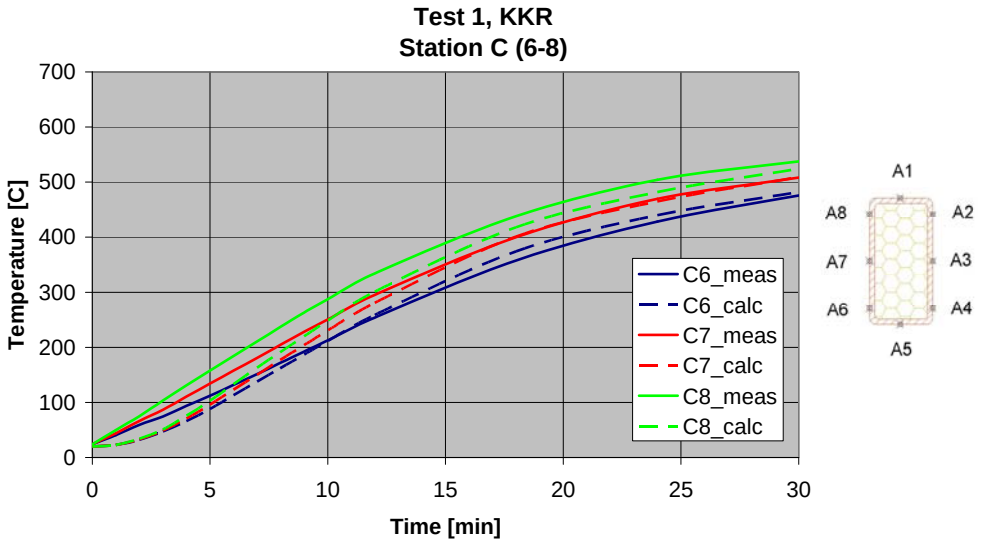

c) Burner side

Figure 45 Measuring station C: Meausured steel temperature and calculated steel temperature at the corresponding positions as a function on time.

Test 2 I-beam, burner in the corner

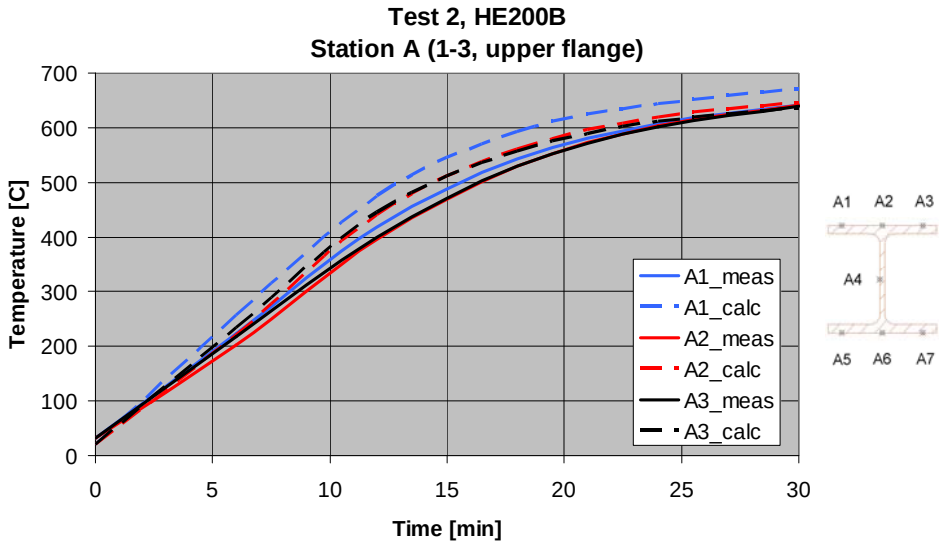

a) Upper flange

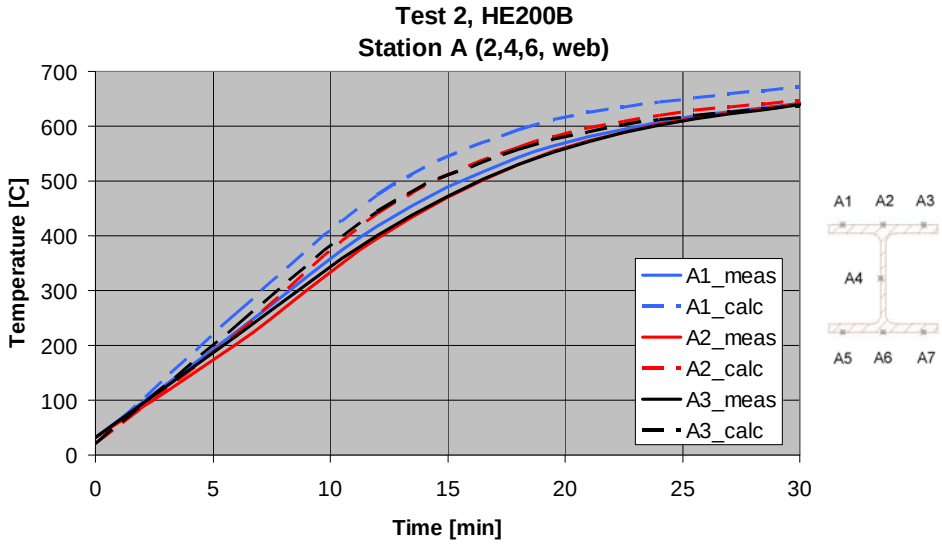

b) Web

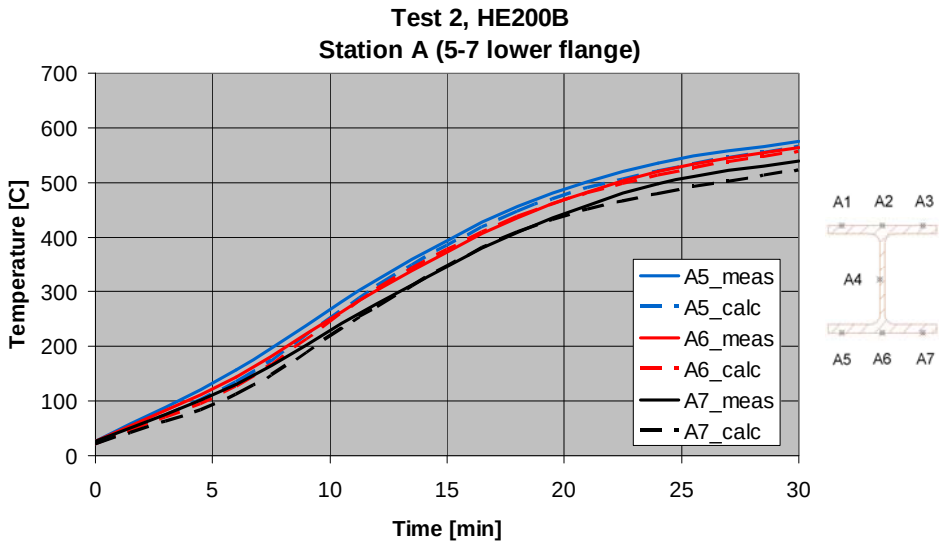

c) Lower flange

Figure 46 **Measuring station A: Meausured steel temperature and calculated steel temperature at the corresponding positions as a function on time.**

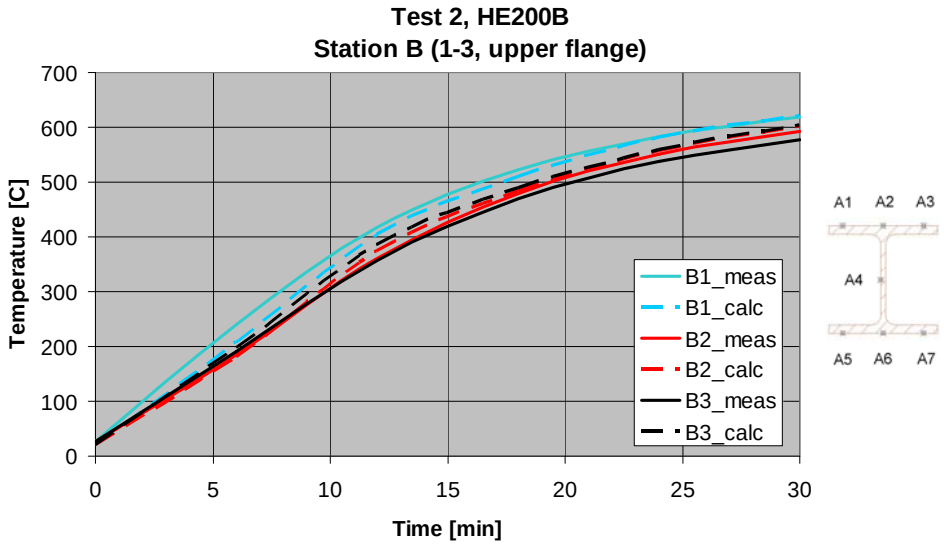

a) Upper flange

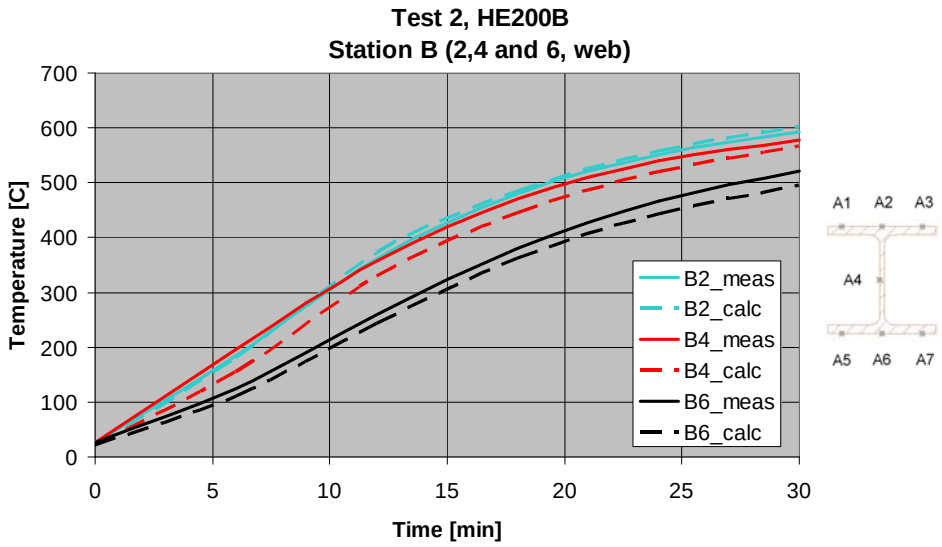

b) Web

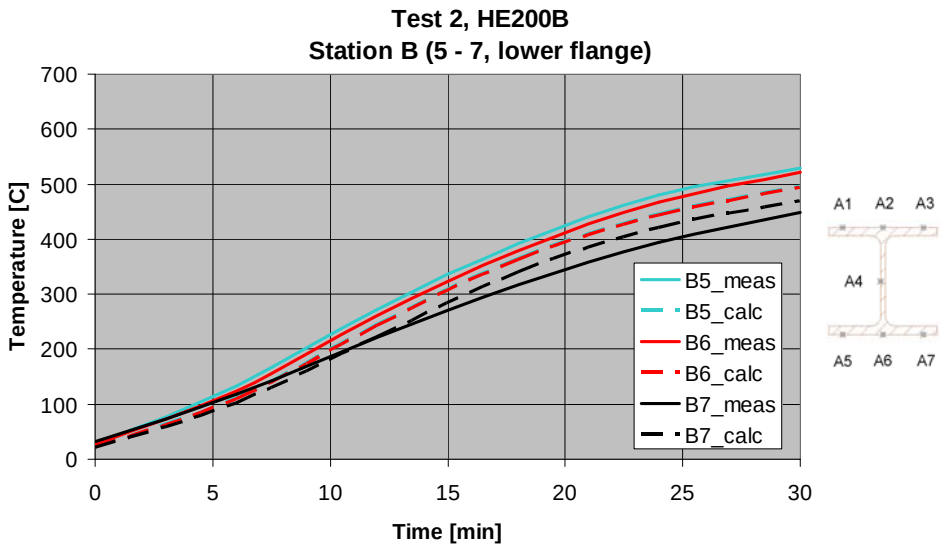

c) Lower flange

Figure 47 Measuring station B: Meausured steel temperature and calculated steel temperature at the corresponding positions as a function on time.

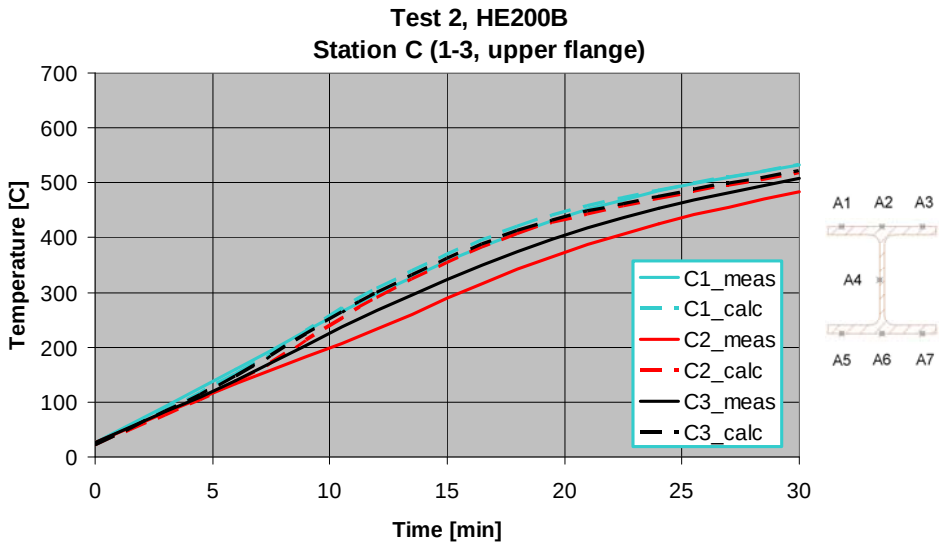

a) Upper flange

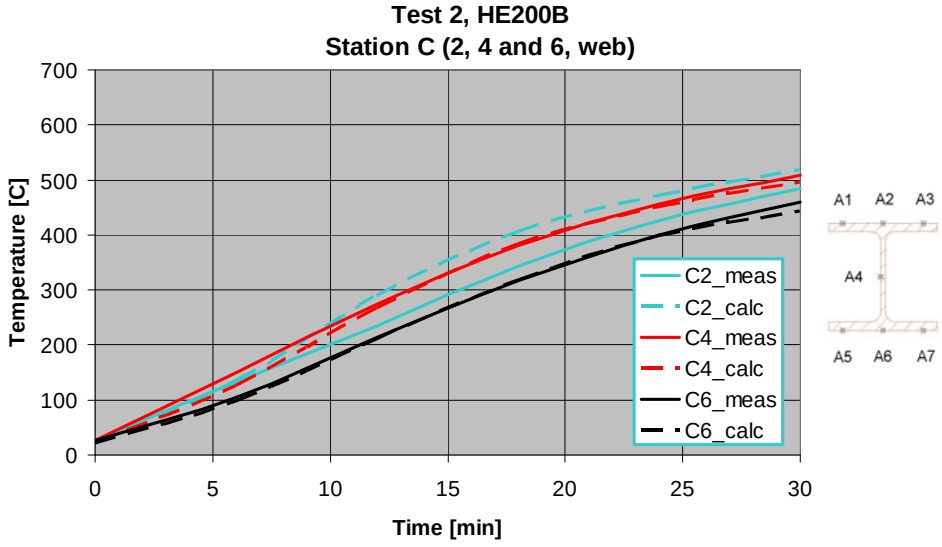

b) Web

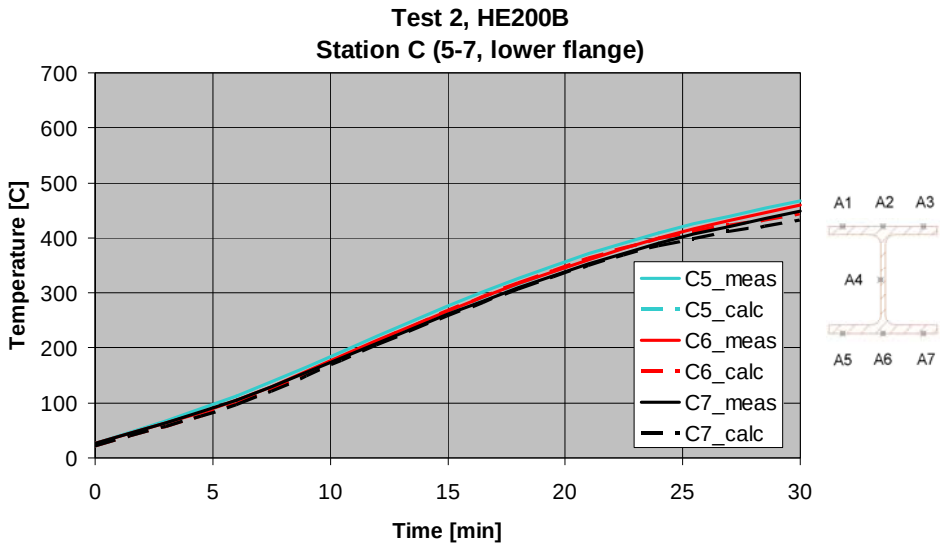

c) Lower flange

Figure 48 Measuring station C: Meausured steel temperature and calculated steel temperature at the corresponding positions as a function on time.

Test 3 I-beam, burner in the centre

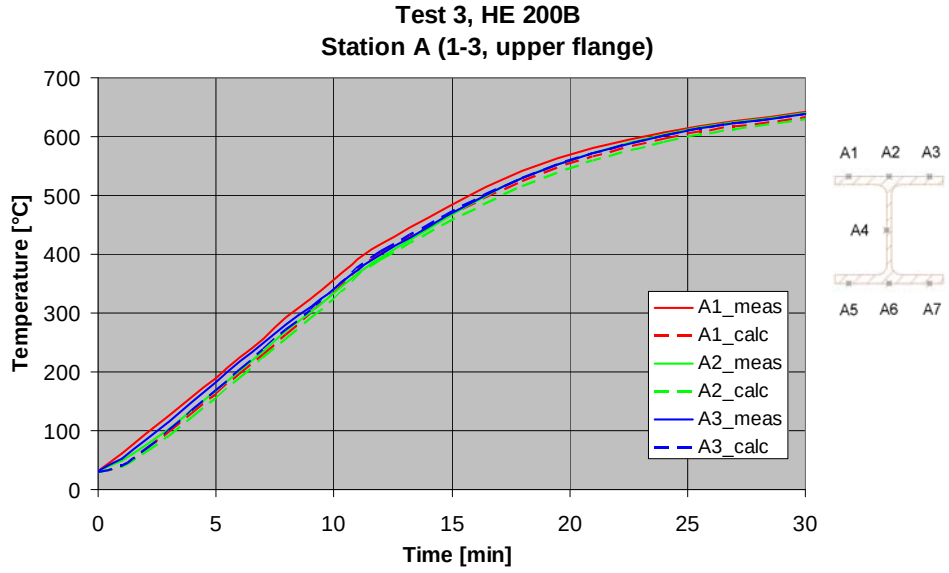

a) Upper flange

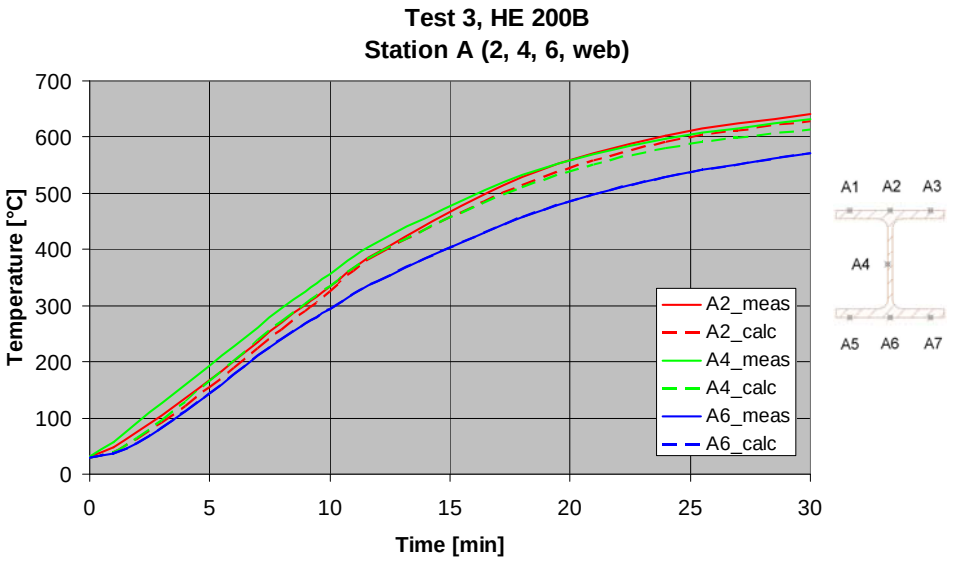

b) Web

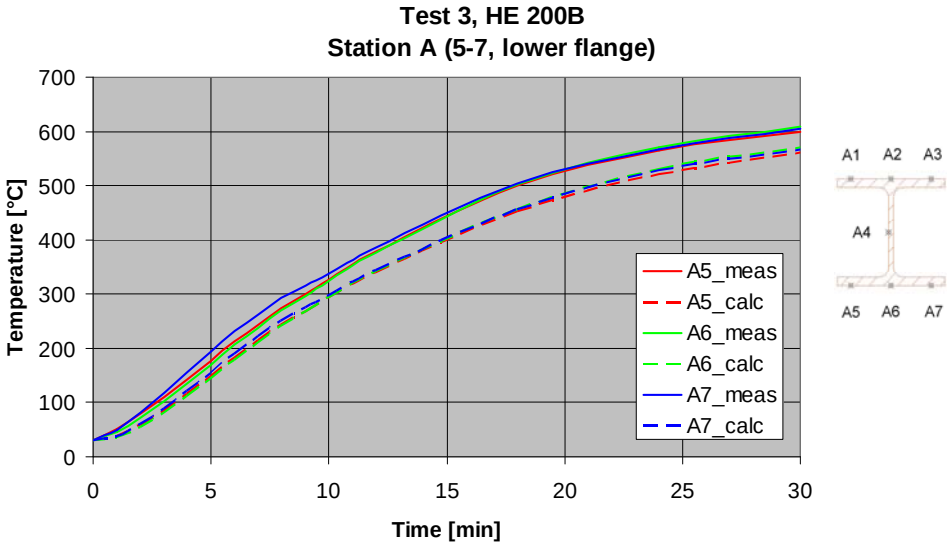

c) Lower flange

Figure 49 **Measuring station A: Meausured steel temperature and calculated steel temperature at the corresponding positions as a function on time.**

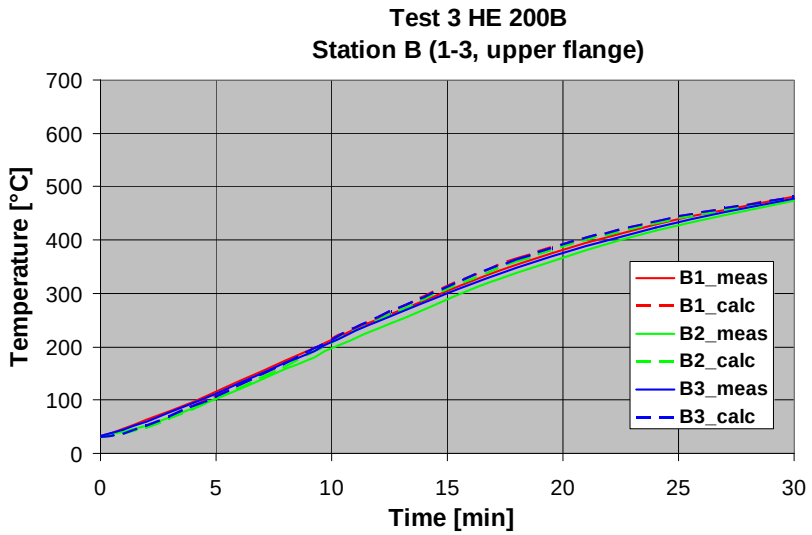

a) Upper flange

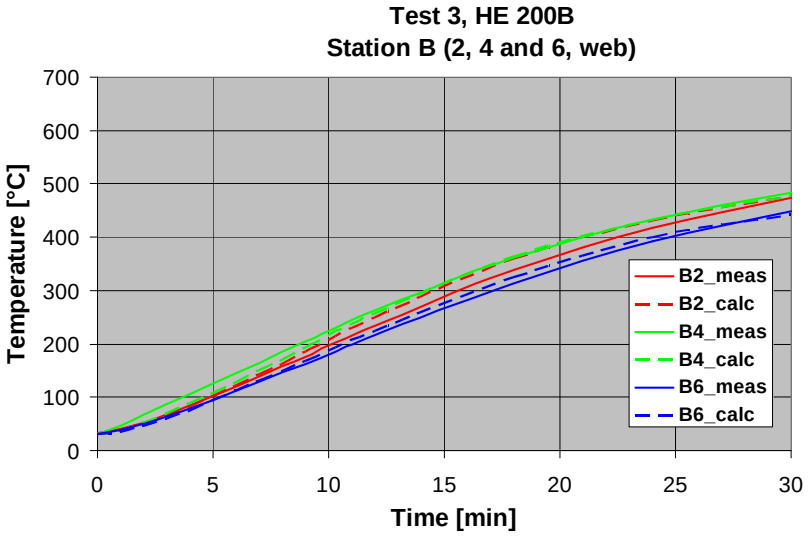

b) Web

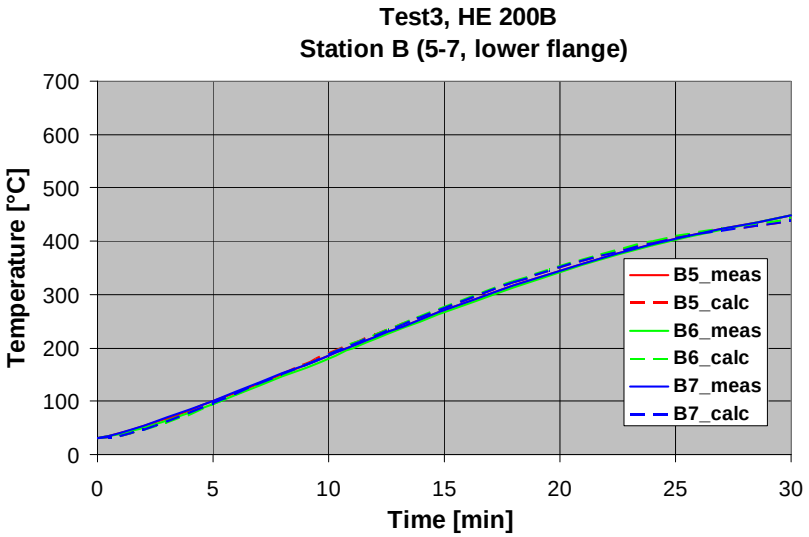

c) Lower flange

Figure 50 Measuring station B: Meausured steel temperature and calculated steel temperature at the corresponding positions as a function on time.

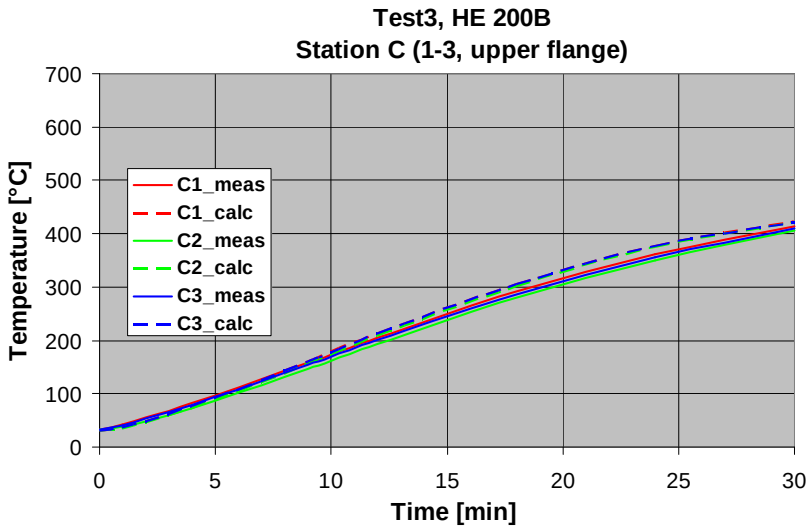

a) Upper flange

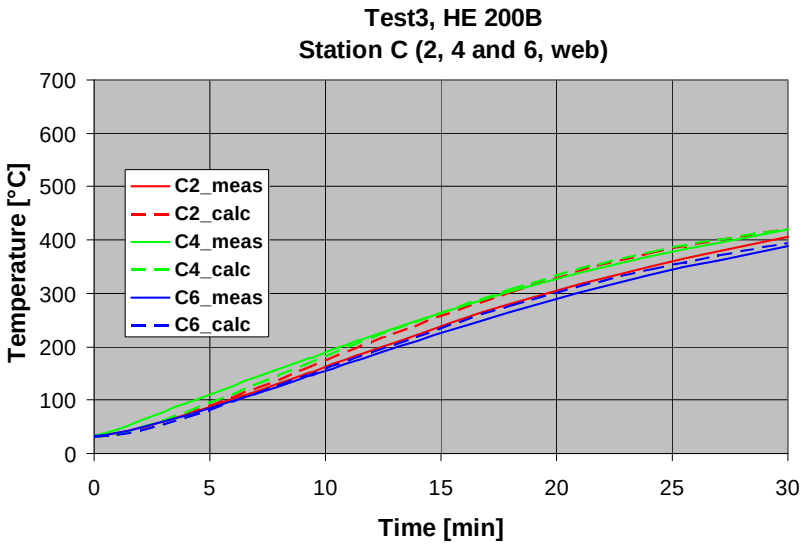

b) Web

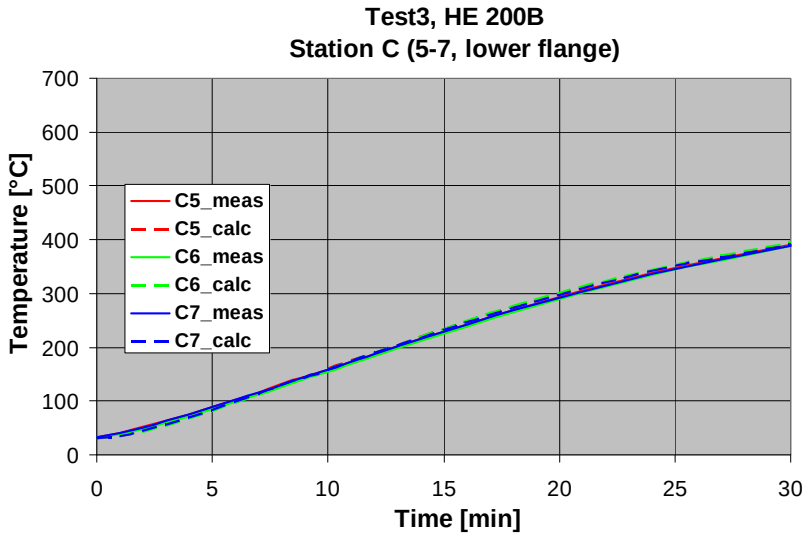

c) Lower flange

Figure 51 Measuring station C: Meausured steel temperature and calculated steel temperature at the corresponding positions as a function on time.

SP Technical Research Institute of Sweden develops and transfers technology for improving competitiveness and quality in industry, and for safety, conservation of resources and good environment in society as a whole. With Sweden's widest and most sophisticated range of equipment and expertise for technical investigation, measurement, testing and certification, we perform research and development in close liaison with universities, institutes of technology and international partners.
SP is a EU-notified body and accredited test laboratory. Our headquarters are in Borås, in the west part of Sweden.

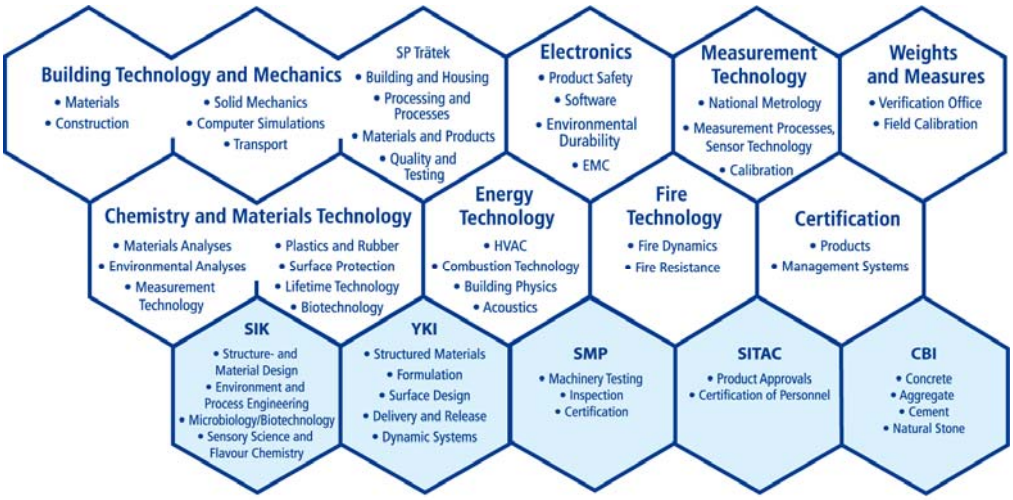

SP is organised into eight technology units and five subsidaries

SP Technical Research Institute of Sweden
Box 857, SE-501 15 BORÅS, SWEDEN
Telephone: +46 10 516 50 00, Telefax: +46 33 13 55 02
E-mail: info@sp.se, Internet: www.sp.se
www.sp.se

Fire Technology
SP Report 2009:19
ISBN 978-91-86319-03-8
ISSN 0284-5172